Chapter 7
Medical Applications of SERS

Abstract The expanding need for noninvasive diagnostics and nondestructive structural analysis led to great progress in SERS medical applications. In this chapter, selected medical in vitro, ex vivo and in vivo applications of SERS from the past decade will be summarized. It involves both intrinsic and extrinsic (SERS tags) detection schemes. In vitro applications include primarily detection of infectious pathogens and cancer diagnostics. In the case of pathogen sensing, the bacterial or viral contamination is detected via their building blocks such as DNA and proteins using hybridization or immunoassays concepts. Cancer diagnostics includes SERS analysis of proteins, nucleic acids, circulating tumour cells, immunophenotyping of cancer cells as well as the detection of various tumour biomarkers produced by cancer cells. The advantages of SERS are the rapid screening, capability of multiplexing and high sensitivity. Glucose monitoring of diabetes will be demonstrated in both in vitro and in vivo conditions. The possibility of introducing metallic NPs or rationally designed NP tags into living cells or living organisms enables many medical applications. Among them in vitro medical therapy, drug release and theranostics along with ex vivo tissue diagnostics and histology will be described. Concerning in vivo applications, Raman imaging for tumour targeting and monitoring of drug release will be primarily highlighted. Finally, clinical SERS applications as guided intraoperative imaging for tumour resection and endoscope-based imaging will be introduced.

7.1 Glucose Sensing In Vitro

The increasing worldwide prevalence of *diabetes mellitus*, which is a major epidemic of this century, requires frequent monitoring of glucose levels of potential patients. Therefore, development of minimally invasive and biologically compatible methods for quantitative glucose detection is needed. SERS is a promising technique for this purpose due to high speed and sufficient sensitivity. In order to be a practicable glucose detection method, SERS must also prove to be accurate and

M. Procházka, *Surface-Enhanced Raman Spectroscopy*,
Biological and Medical Physics, Biomedical Engineering,
DOI 10.1007/978-3-319-23992-7_7

reliable in the clinically relevant concentration range and in complex biological fluids. Glucose concentration over 100 mg dl^{-1} in blood is indicative of a prediabetic conditions and concentration higher than 126 mg dl^{-1} (7.0 mM) generally results in a diagnosis of diabetes. SERS is sensitive enough for this concentration range. Moreover, SERS is compatible with aqueous solutions and Raman spectral characteristics can avoid possible interference of other molecular species. A large challenge, however, is the poor adsorption of glucose to bare silver or gold substrates.

Specific analytical label-free SERS biosensor for glucose was designed by using of suitable functionalized Ag FON or Au FON substrates (described in Sect. 3.4.4) by the Van Duyne group (Haynes et al. 2005; Yonzon et al. 2006). The diameter of used nanospheres and the thickness of metal layer were optimized for a particular excitation wavelength. The substrates were functionalized with SAMs and an additional alumina layer of about 1 nm thickness. Implementing a partition layer between metal surface and analyte has three advantages for Ag surface: (i) protection it from oxidation; (ii) improvement of its stability and (iii) tailoring it by choosing appropriate SAMs to selectively bind analyte of interest. The SAMs of decanethiol (DT) on Ag FON substrate (Shafer-Peltier et al. 2003) functioned as a partition layer that concentrates glucose near the Ag FON surface enabling it to be detected at concentrations lower than 5 mM. To further improve the performance of partition layer glucose sensors, a mixed SAM monolayer of DT and mercaptohexanol (DT/MH), was formed on an Ag FON and employed for real-time sensing (Lyandres et al. 2005). The DT/MH monolayer was shown to be stable for 10 days and was used as a partition layer for quantitative analysis of glucose with less calibration error than previous SAMs. Moreover, this sensing strategy was successfully applied for real-time detection of physiological glucose concentrations (0–450 mg dl^{-1}) in bovine plasma. In a flow cell setup, the authors demonstrated glucose sensing and departitioning with time constants of 25 and 28 s, respectively (Lyandres et al. 2005). Later, accurate glucose detection was possible over a larger concentration range (10–800 mg dl^{-1}, 0.5–44 mM), making this sensing strategy applicable to a more diverse set of diabetes patients (Stuart et al. 2005).

The novel glucose biosensor using (Ag@Au NPs)/(graphene oxide) nanostructures functionalized with mercaptophenylboronic acid has been reported (Gupta et al. 2013). The assay was based on the ability of glucose to form a bidentate glucose-boronic complex while most of the other physiologically relevant carbohydrates bind to boronic acid as monodentate complexes. The biosensor was successfully applied for the determination of glucose in blood samples. The concentration of glucose was determined to be 1.970 mM with high precision from measurements repeated six times (Gupta et al. 2013). The same approach was applied to determine glucose concentration in urine samples (Kong et al. 2013). The scheme of sensor is depicted in Fig. 7.1. Sensor was formed by a sandwich assay in conjunction with a metal carbonyl probe. Two carbohydrate receptors were used; the first (primary) receptor was 4-mercaptophenylboronic acid anchored onto a SERS substrate and the second (secondary) receptor was a 4-mercaptophenylboronic acid–triosmium carbonyl cluster conjugate (Os–BA). Glucose was first captured by the

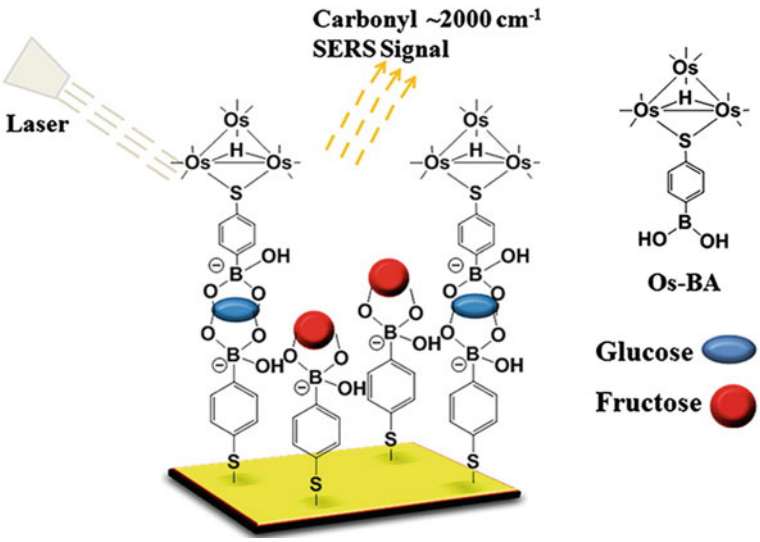

Fig. 7.1 Glucose sensor. A glucose molecule brings 4-mercaptophenylboronic acid-triosmium carbonyl cluster conjugate (Os–BA) to the substrate via formation of a bidentate complex. The *short lines* extending from Os represent carbonyl (CO) ligands (adapted with permission from Kong et al. 2013. Copyright 2013 American Chemical Society)

primary carbohydrate receptor and then labelled with the Os–BA. In this way, it was possible to selectively quantify the concentration of glucose via the SERS band of CO stretching vibration of the metal carbonyl $\sim$2000 cm^{-1} which lies far from possible interference with spectral bands of other biomolecules. Os–BA possesses a much greater affinity for glucose than for fructose and galactose. The SERS-active substrate in this study was bimetallic Ag/Au FONs. In a pilot experiment, the concentration of glucose in the urine sample was determined to be 5.1 mM, which was in agreement with the amount of added glucose (5.0 mM), but LOD was even less (0.1 mM). In comparison to other glucose detection methods, this assay exhibited several advantages: (i) no prior purification of the sample was needed, (ii) an extremely low sample volume was required and (iii) it showed very high specificity for glucose.

7.2 Pathogen Sensing In Vitro

The rapid screening of pathogens remains an issue in food safety, public health assurance and diagnosis of infectious diseases. The bacterial or viral contamination is detected via their building blocks such as DNA and proteins. Routine analyses of pathogens typically involve time-consuming (several days) biochemical characterization of cultured bacteria taken from contaminated sources. Advances in SERS

analysis using SERS tags offer possibilities for rapid screening and detection. SERS analyses include pathogen NA identification via NA hybridization scheme, immunoassays detecting specific protein pathogen biomarkers and direct diagnosis of bacteraemia as well as UTI from body fluids.

7.2.1 Pathogen Sensing Using NA Hybridization

The main approach of pathogen sensing is identification of pathogen NA sequence. Owing to the small content of DNA in cells and its structural complexity, its analysis requires denaturation (heat), fragmentation (restriction endonucleases), separation (electrophoresis), amplification (PCR) and detection (quantitative PCR or microarray techniques). The advantages of SERS are the capability of multiplexing and high sensitivity. The detection scheme is based on hybridization which was described in Sect. 5.2.2. Synthetic oligonucleotides labelled with dye form SERS probes to proper identification of pathogen sequence complementary to the probe. The PCR can be used to simultaneously amplify the specific target DNA sequences enabling amplification of sensitivity of pathogens (Isola et al. 1998).

First SERS gene probe based on hybridization of labelled target sequence has been developed for the selective detection of human immunodeficiency virus (HIV) on Ag islands as SERS-active surface (Vo-Dinh et al. 1994). The effectiveness of such detection scheme was later improved by PCR amplification (Isola et al. 1998). The primer labelled with cresyl fast violet was used for PCR amplification of the 93-base pair target sequence (HIV *gag* gene). The capture probe sequence was bound to PS and hybridized with the total PCR product. Only the amplified target sequence hybridized with the capture probe sequence provided SERRS signal of cresyl fast violet (Isola et al. 1998). Later, a subattomolar HIV-1 DNA detection assay based on multilayer metal-molecule-metal nanojunctions was developed (Hu et al. 2010). First, label-free target DNA facilitated the precipitation of "detection unit I" on the substrate through forming a sandwiched structure based on the capture probe. It results in the first level amplification of the target. Following that, the binding site on "detection probe I" was further recognized by "detection unit II". These two complementary probes served as bricks to build up the metal-molecule-metal nanojunctions between Au NPs that not only created SERS "hot spots" between Au NPs, but also obviously decreased the distance between Au NPs and Raman labels. Therefore, the SERS signal of the tag molecules on these detection probes was significantly enhanced. Such a platform was able to detect a HIV-1 DNA sequence at concentration as low as 10^{-19} M with the specificity of single base mismatch discrimination (Hu et al. 2010). In a multiplex assay (depicted in Sect. 5.2.5), six commercially available dyes—Cy3, Cy3.5, Cy5, TAMRA, texas red and RH6G—were conjugated to different oligonucleotide sequences specific for six different targets including several viruses (Cao et al. 2002). For hybridization, the target DNA and the Au SERS probes were first sequentially added to the chip functionalized with the corresponding capture

sequence. Next, SERRS enhancement for detection of the hybridization event was performed by the reduction of silver ions with hydroquinone. Such sandwich system allowed SERS detection of specific sequences, effectively discriminating between single nucleotides of Hepatitis A, Hepatitis B, HIV, Ebola and Variola viruses. Sufficient correlation between the oligonucleotide sequence and the corresponding SERRS spectrum of the dye attached to it was excellent and LOD of 20 fM was obtained.

An experimental setup to detect dengue (the most common mosquito-borne global disease) virus sequences by SERS on-a-chip was invented. A microfluidic SERS assay was based on synthetic DNA sequences that mimic viral dengue serotypes and TAMRA-labelled targets. The complementary capture probes were immobilized on Au NPs and the SERS measurement was performed within the optofluidic SERS-chip (Huh et al. 2009). Marotta and co-workers reported a label-free detection of DNA hybridization using short oligonucleotides (less than 9 base pairs) for the analysis of the respiratory syncytial virus responsible for lower respiratory tract infections (Marotta et al. 2013). An assay consisted of an array of 5′-thiolated ssDNA oligonucleotides immobilized on the Ag NR surface. It served as capture probes for the detection of synthetic RNA sequences coding for a genetic mutation in the influenza PB1-F2 protein (Negri and Dluhy 2013). Hybridization of the DNA probes to their complementary RNA sequences was detected using SERS. HCA procedure was able to distinguish with 100 % accuracy the spectra of the complementary DNA probe–RNA target from the spectra of the immobilized DNA probes alone, or the DNA probes incubated with complementary RNA sequences, which are not complementary. LOD of such immunoassay was about 10 nM which is 10× lower than standard ELISA.

Molecular sentinel (MS) is a very interesting concept of SERS-based DNA detection (Wabuyele and Vo-Dinh 2005). Figure 7.2 shows the principle of the MS detection strategy. The MS consists of a DNA probe sequence that has a SERS label at one end and a metallic NP attached to the other end via a thiol group. The middle section of DNA probe sequence contains a sequence complementary to the target sequence to be detected and two arms that have complementary sequences in order to form a hairpin loop configuration under normal conditions. The hairpin loop configuration is designed so that the SERS label is in contact or in proximity (<1 nm) to the metallic NP, which induces a strong SE(R)RS signal of the label. SERS signal from the label is detected when the probe is in the closed hairpin state. Hybridization with complementary sequence causes the hairpin opening and thus separation of the label and the metallic NP, which leads to decrease of SERS signal. This concept does not need the target sequences to be labelled.

To demonstrate the feasibility of the MS as a SERS diagnostic tool, the Vo-Dinh group introduced GeneAmplimer HIV-1 control reagents having *gag*-specific primers SK38 and SK39 to amplify a 115-bp HIV-1 *gag* fragment (Wabuyele and Vo-Dinh 2005). The PCR amplicons of retroviral DNA template were hybridized with the SERS nanoprobe—SK 19 MS—incorporating a partial sequence for the HIV-1 *gag* gene and detected using the SERS MS approach. Later, the same group reported SERS MS to detect the human radical S-adenosyl methionine domain

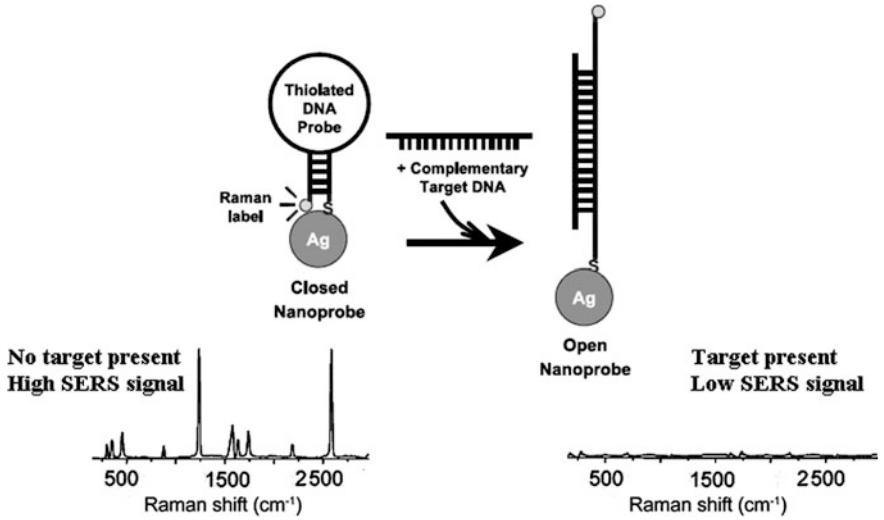

Fig. 7.2 Signalling concept of SERS molecular sentinels (MS). Strong SERS signal is observed when the MS nanoprobe is in the hairpin closed conformation (which is in the absence of target DNA). SERS signal is diminished in the presence of the target DNA which causes opening of MS (adapted with permission from Wabuyele et al. 2010. Copyright 2010 Springer)

containing 2 (RSAD2) RNA target (Wang et al. 2013a). The human RSAD2 gene has recently emerged as a novel host-response biomarker for diagnosis of respiratory infections. The results showed that the RSAD2 MS nanoprobes exhibited high specificity and could detect as low as 1 nM target sequences. The human samples were used in their preliminary tests and the authors suggested the system could be further developed into a portable lab-on-a-chip device. It could measure multiple genome-derived markers for rapid diagnosis of infectious diseases caused by viruses at the point of care. Recently, LOD 2.67 aM for the RNA genetic marker associated with influenza virus was reported (Pang et al. 2014). The assay consisted of an array of Raman label tagged hairpin-DNA (MS reporter) immobilized on metallic FON SERS substrate. The sensing process only required a single hybridization step and post-hybridization washing as well as PCR amplification steps were not necessary.

Concerning bacterial pathogens, a triplex scheme was successfully applied to detect three mixed oligonucleotide probe sequences of different *Escherichia coli* bacterium variants. This was the first multiplex SERRS detection using oligonucleotides labelled with 3 different dyes in a microfluidic system (Docherty et al. 2004). Later, the multiplex system consisting of the oligonucleotides labelled with 5 different dyes (at concentration 1.82×10^{-9} M) was applied in situ (Faulds et al. 2007). Moreover, two different excitation wavelengths enabled to optimize the resonance of a particular dye and consequently to maximize its SERRS signal. The same group reported multiplexed detection of several *Escherichia coli* strains by

using 5 different dye labels and multivariate analysis to better distinguish between the SERS signals of five labels. The ability to discriminate the presence or the absence of a particular label in the mixture was achieved with sensitivity, specificity, accuracy and precision between 0.98 and 1 (Faulds et al. 2008). MacAskill and co-workers developed an easy SERRS assay to monitor simultaneously three DNA sequences from methicillin-resistant bacterium *Staphylococcus aureus,* common hospital contamination (MacAskill et al. 2009). The principle is that ssDNA is adsorbed more readily to Ag NPs treated by spermine to overcome electrostatic repulsion than dsDNA. Possible hybridization event is taking place before adsorption to Ag NPs. If only nontarget DNA was present, the dye-labelled DNA was free to be adsorbed on the Ag NPs and provided a strong SERRS signal. The presence of target DNA allowed the hybridization and formation of dsDNA which cannot be adsorbed onto the Ag surface resulting in a reduction of the SERRS signal.

A positive homogeneous assay, very similar to MS designed by Wabuyele and Vo-Dinh (Wabuyele and Vo-Dinh 2005), was developed by van Lierop and co-workers (van Lierop et al. 2011). The assay utilizes specifically designed self-complementary primers labelled with a SERS-active dye. In contrast to MS, the high SERS signal of dye is obtained in the presence of target DNA which opened the primer through preferential binding, resulting in a region of labelled ssDNA remaining free to adsorb onto the NP. On the other hand, SERS signal is diminished in the absence of target DNA when the primer stayed closed. Highly intense SERS signals were obtained after addition of genomic DNA from *Staphylococcus epidermis* demonstrating the possibility for the detection of multiple targets in clinical samples (van Lierop et al. 2011). Later, the same group improved SERS assay using PCR and enzyme digestion to generate dye-labelled ssDNA and to detect *Staphylococcus aureus* pathogens (van Lierop et al. 2013).

Harper and co-workers employed a combination of TaqMan assay in which signal is generated through enzymatic probe cleavage and SERS to detect DNA of a *Staphylococcus aureus* (Harper et al. 2012). TaqMan assay is based on the 5′-to 3′-exonuclease activity of the thermostable enzyme *Thermus aquaticus* (Taq) polymerase to simultaneously amplify the template and digest the TaqMan probe. The LOD of DNA of a *Staphylococcus aureus* was lower than for conventional fluorescence detection and clinically relevant samples were detected with high specificity. Graham and co-workers introduced another sandwich hybridization assay based on oligonucleotide-NPs conjugates with enhanced stability for the assembly-based detection of *mecA* gene of *Staphylococcus aureus* (Graham et al. 2011). In typical experiment, Au NP or Ag NP conjugates functionalized with two different, noncomplementary oligonucleotides, hybridized upon addition of target oligonucleotide. The molecular recognition event and the formation of structured NP assemblies caused a visual colour change in the NP suspension.

Kang and co-workers developed a Au NP-on-wire SERS sensor for multiplex pathogen DNA detection (Kang et al. 2010). The sensor is illustrated in Fig. 7.3. Au NWs (150 nm diameter) were functionalized with thiolated captured sequences on the Si substrate and incubated with target sequences. Then, such functionalized Au

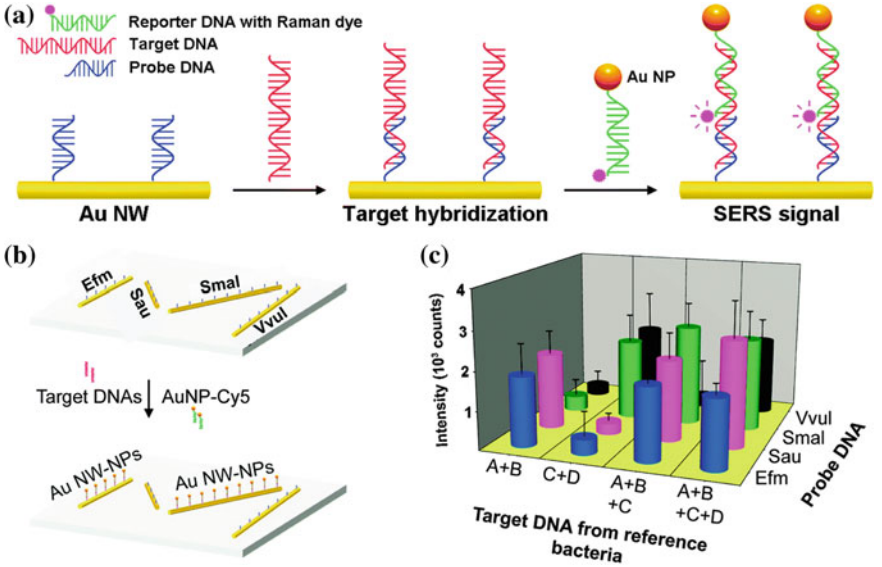

Fig. 7.3 Au NP-on-wire SERS sensor for multiplexed pathogen DNA detection. **a** Scheme of the target DNA detection. **b** Scheme of multiplex approach for detection of DNA extracted from four bacteria. **c** SERS intensities of the RRM when sample contains different kinds of target DNA. *A* Efm: *Enterococcus faecium*; *B* Sau: *Staphylococcus aureus*; *C* Smal: *Stenotrophomonas maltophilia*; *D* Vvul: *Vibrio vulnificus* (adapted with permission from Kang et al. 2010. Copyright 2010 American Chemical Society)

NWs were immersed into a suspension of the reporter DNA-functionalized Au NPs to form Au particle-on-wire structure via sandwich hybridization of probe-target-reporter sequences (Fig. 7.3a). Thus, SERS "hot spots" were created at the gaps between the Au NW and the Au NPs. Strong SERS signals from RRM (Cy5) on the reporter sequences were observed only when the complementary target sequences were added, indicating a high specificity to DNA sequences. A multiplexed pathogen DNA detection platform was constructed by Au NWs attached to different probe sequences, respectively, on a single Si substrate. Four different Au NWs were first functionalized with probe DNA corresponding to the four targets. These NWs were then hybridized with the target DNA, followed by incubation with reporter DNAs with Cy5 at 5′-terminus and Au NP at 3′-terminus (Fig. 7.3b). Identification of DNA sequences extracted from four pathogenic strains, *Enterococcus faecium, Staphylococcus aureus, Stenotrophomonas maltophilia* and *Vibrio vulnificus* (responsible for severe human diseases like sepsis or gastroenteritis) was possible with very low LOD (10 pM). Figure 7.3c shows SERS intensities of 1580 cm^{-1} band (corresponding to the RRM—Cy5) when the sample contains two, three and four kinds of target DNAs of concentrations 10^{-8} M each.

Hybrid MNPs for the enrichment of the target molecules and consequently for the increased detection sensitivity were also employed in pathogen DNA detection in a hybridization scheme. For example, the *omp*A gene of *Chlamydia trachomatis* which is a sexually transmitted bacterium, was detected using a SERS assay based on MNPs (Dougan et al. 2011). Spermine hydrochloride served to promote adsorption of oligonucleotides on the NP surface. A sandwich-hybridization was performed with a magnetic bead immobilized capture probe, the target DNA and terminal phosphate/TAMRA-modified reporter probe. Strelau and co-workers reported a novel approach for the sequence specific detection of DNA using MNPs to amplify PCR products (Strelau et al. 2011). To achieve fast and efficient binding, the hybridization procedure was performed in solution. A streptavidin-modified MNPs, biotin-labelled capture DNAs and probe oligonucleotides carrying a RRM were used. SERS substrate was generated by enzyme-induced growth of Ag NPs and the SERS label attached to the probe DNA was detected. To further purify and enrich the DNA strands of interest, MNPs served for their separation. The system was applied to detect PCR products amplified from DNA of specific agents of epizootic diseases. Sequences of the bacterium *Mycoplasma mycoides* subspecies *mycoides* small colony type (causing contagious bovine pleuropneumonia) were used as PCR targets. To demonstrate the multiplex capability of SERS, the simultaneous detection of three different PCR products labelled with three dyes (Cy3, FAM and TAMRA) was performed (Strelau et al. 2011). MNPs also served in sandwich hybridization assays of synthetic target DNA of the West Nile virus producing West Nile fever and encephalitis (Zhang et al. 2011). The Au NPs and iron MNPs were employed for capturing the target DNA, instead of flat solid substrates commonly used in conventional SERS assays for DNA detection. Figure 7.4 shows the detection method for the West Nile virus target DNA. DSNB served as both the RRM and the linker for the reporter sequence. The hybridization reactions were incubated for a short period. Hybridized complex was formed by a capture substrate, a target oligonucleotide and a SERS label. After the hybridization event, an external magnet served to concentrate hybridized complexes within the focus of laser beam for SERS measurement. This approach reached a LOD 10 pM for West Nile virus target DNA.

7.2.2 Pathogen Sensing Using Immunoassays

Immunoassay platforms, where metallic NPs are functionalized with antibodies or aptamers that recognize target biomolecules on the surface of the pathogen, represent another approach to detect pathogens. The main principles of immunoassays have been explained in Sect. 5.3.3.

Knauer and co-workers reported the label-free SERS detection of *Legionella pneumophila* and *Salmonella typhimurium* cells in water (Knauer et al. 2010). The total assay time was only 65 min. The bacterial suspension was incubated on a glass chip containing the respective antibodies. After the cells were captured and

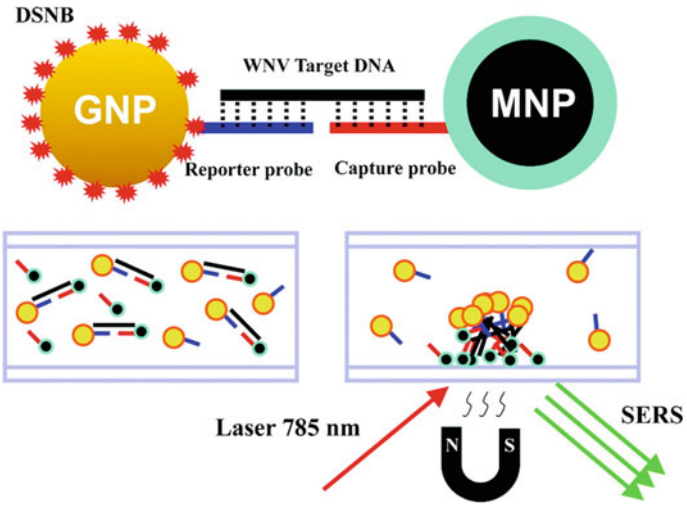

Fig. 7.4 SERS detection of West Nile virus target DNA using MNPs as capture substrates. DSNB served as both the RRM and the linker for the reporter sequence, *GNP* gold nanoparticle, *MNP* magnetic nanoparticle, *WNV* West Nile virus. The hybridization complex was separated and concentrated within the focus beam of the laser by magnetic pull-down and detected by SERS (reproduced with permission from Zhang et al. 2011. Copyright 2011 American Chemical Society)

immobilized on the glass chip, the chip was placed on a polycarbonate tray which was filled with Ag colloid. Sodium azide served for specific agglomeration of the Ag NPs at the bacterial cell wall resulting in a significant SERS signal enhancement. Reliable identification of the bacteria was possible by means of their fingerprint spectra containing mostly strong peaks of amide I, II and III of peptides. Concentrations between 10^6 and 10^9 cells per ml were examined for *Salmonella typhimurium* and between 10^8 and 10^9 cells per ml for *Legionella pneumophila*. SERS spectra obtained from several cells of the same colony provided good reproducibility. In other studies, immunoassays based on labelled SERS tags were employed. Au NPs coated with anti-protein A and RRM (5,5′-dithiobis-2-nitrobenzoic acid) were used for identification of *Staphylococcus aureus* via specific binding of functionalized SERS tag to the bacterial surface antigen. LOD of 1 pg ml^{-1} of protein A was achieved this way (Lin et al. 2008). Similarly, 500 *Mycobacterium avium* subspecies *paratuberculosis* per ml were detected in milk (Yakes et al. 2008). The simultaneous detection of three different bacteria was realized by using Au, Ag and Ag/Au nanoshell NPs immobilized with anti-*Salmonella typhimurium* aptamers, anti-*Staphylococcus aureus* and anti-*Escherichia coli* O157:H7 antibodies, respectively, and unique RRMs (Ravindranath et al. 2011). Here, a microfiltration step was applied to consolidate a highly selective and specific detection platform with total detection time under 45 min and LOD ranging between 10^2 and 10^3 colony forming units per ml.

The possibility of separation and detection of multiple pathogens in a food matrix by using magnetic SERS tags has also been reported (Wang et al. 2011a). In this work, pathogens were first immunomagnetically captured with MNPs and then pathogen-specific SERS tags were functionalized with corresponding antibodies to allow the formation of a sandwich assay. The detection of multiple pathogens in selected food matrices was achieved by changing the RRM on the SERS tags. *Salmonella enterica* serovar *Typhimurium* and *Staphylococcus aureus* were chosen to demonstrate the possibility of multiple pathogens detection. The lowest cell concentration detected in a spinach solution was 10^3 colony forming units per ml. The results of a blind test in peanut butter validated that this LOD was achieved with high specificity.

7.2.3 Direct Bacterial Identification in Human Body Fluids

Bacteraemia, the presence of bacteria in the patient's blood, resulting from severe infections in the body, surgical wounds, or contaminated implanted devices may lead to a sepsis. Its onset is very fast. The current standard testing methods in hospitals are based on cultivation bacteria. However, this procedure normally takes up to 3 days. Therefore, the big advantage of SERS is the speed of identification. Effort is made to improve SERS detection of pathogens in human body fluids using portable Raman microscopes, robust metallic substrates and by a simplification of sample preparations (Premasiri et al. 2012b, 2014).

The SERS diagnostics based on direct analysis of blood samples requires a detail SERS study of whole blood. SERS spectra of whole human blood, plasma and red blood cells were reported for the first time by Premasiri et al. (2012a). They used small aggregates (2−15 NPs) of monodispersed Au NPs (80 nm diameter) covering the outer layer of $\sim$1 mm^2 SiO_2 substrate. The freshly drawn blood sample was refrigerated (8 °C) prior to SERS measurements. For SERS experiment, the blood sample ($\sim$1 µl) was placed on the Au substrate to form only a thin film. The SERS spectra of fresh whole human blood and fresh plasma, observed $\sim$1 h after being drawn are compared in Fig. 7.5, spectrum b and c, respectively. The spectra look very similar showing strong vibrational bands at 490, 639, 895, 1134, 1362, 1569 and 1649 cm^{-1}. The NRS spectrum of dried whole blood (spectrum a) is very different. The authors concluded that the NRS spectrum of whole blood shows exclusively the spectral features of haemoglobin while SERS spectrum is due to blood components other than haemoglobin. Moreover, the SERS spectra of the same blood sample stored at 8 °C undergo significant evolution as a function of storage time over a period of 24 h. For example, new vibrational bands at 724, 965, 1070, 1332, 1365 and 1453 cm^{-1} appeared and increased in relative importance as a function of whole blood storage time. All the changes were attributed to hypoxanthine and SERS spectrum of whole blood stored for $\sim$24 h was essentially that of hypoxanthine.

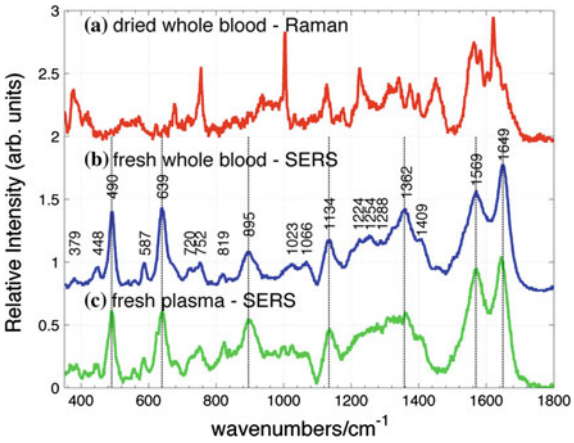

Fig. 7.5 Raman spectra of whole blood samples. **a** NRS spectrum of dried whole blood, **b** SERS spectrum of fresh whole blood, **c** SERS spectrum of fresh plasma. 785 nm excitation wavelength (reproduced with permission from Premasiri et al. 2012a. Copyright 2012 American Chemical Society)

In practice, the problem of diagnosis of pathogen bacteria from a blood sample is that the relative concentration of bacterial cells (only 10^3 per ml) in the infected blood of patients is much smaller than of blood cells (10^9 per ml). Premasiri and co-workers developed an automated selective lyses, centrifugation and micro-evaporation procedure to achieve the required enrichment $\sim 10^5$ of bacterial cells to observe their SERS spectra. It allows acquisition of SERS spectra in 100 nl volumes of infected blood (Premasiri et al. 2014). Since only relatively subtle distinctions are often observed between the SERS spectra of samples containing various pathogens, the empirical algorithm based on the SERS intensity or particular bands does not provide a sufficient diagnostic sensitivity and specificity. Therefore, the PCA approach was applied to determine the reproducibility and specificity of the diagnosis derived from SERS spectra (Patel et al. 2008). The PCA procedure involves removing the high frequency noise by Fourier filtering and conversion of SERS spectrum into a barcode, which is of "ones" or "zeros" based on the sign of the second derivative of the spectrum as a function of Raman frequency. The best clustering results derived from the SERS bacterial spectra are consistently obtained when second-derivative-based barcodes are used as input vectors for the PCA treatment. When barcodes are assigned on the basis of the sign of the second derivative, i.e. 1 for upward curvature (positive second derivatives) and 0 for downward curvature (negative second derivatives), each species is represented by a frequency-dependent binary fingerprint. A threshold for zero, usually set at about 10 % of the maximum value of the second derivative, is used to determine a minimum value for a 0 bit assignment for this barcode. This threshold helps discriminate against residual noise components. Such second-derivative barcodes for the two closely related *Bacillus* bacteria (*Bacillus antracis Sterne* and *Bacillus thuringiensis*) are shown in Fig. 7.6a as an example. The barcodes were the

inputs for the PCA analysis. Figure 7.6b shows barcode PCA plots for four *Bacillus* bacteria spiked and recovered from human blood. Black lines are equidistant to the mean of each cluster (Premasiri et al. 2014). The barcode methodology resulted in significantly enhanced diagnostic specificity.

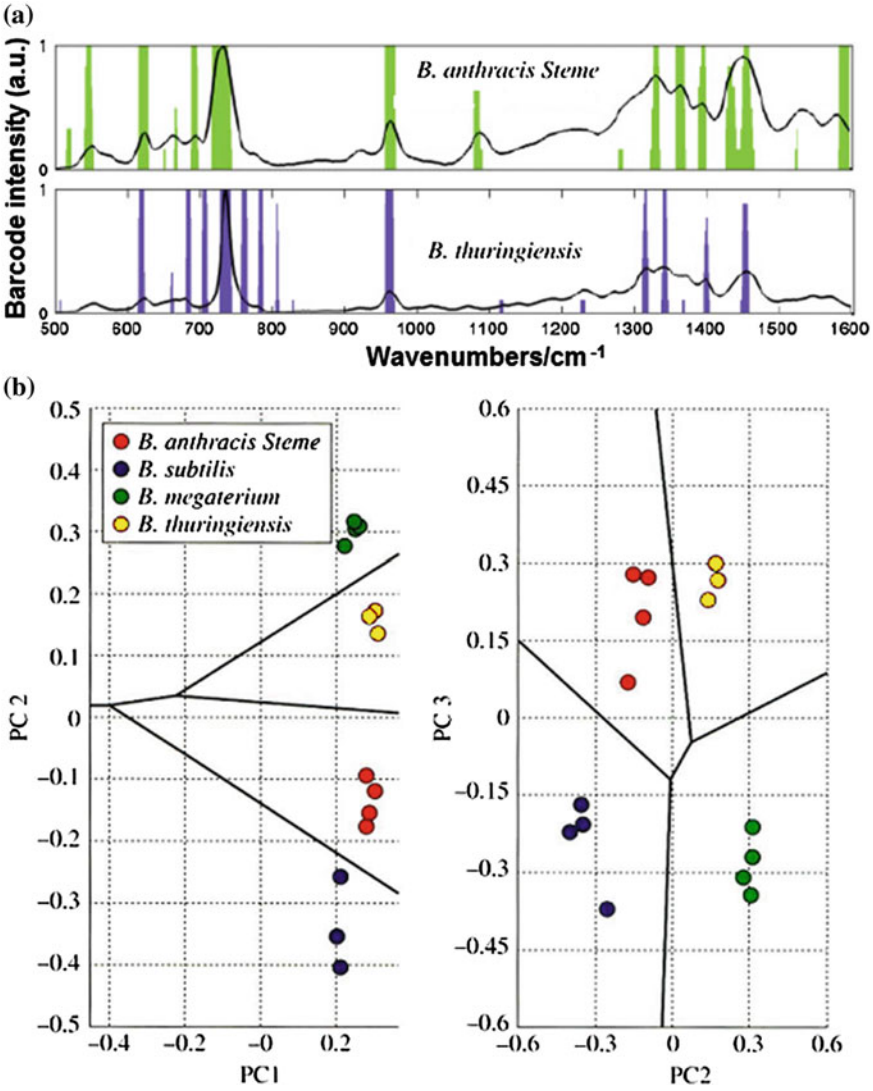

Fig. 7.6 Pathogen bacteria SERS detection from blood samples. **a** Second-derivative barcodes for the two closely related *Bacillus* bacteria. **b** Barcode-based PCA analysis of four *Bacillus* bacteria spiked and recovered from human blood. *Black lines* are equidistant to the mean of each cluster (**a** adapted with permission from Patel et al. 2008, **b** adapted with permission from Premasiri et al. 2014. Copyright 2008, 2014 John Wiley & Sons, Ltd)

The first SERS analysis of clinical bacterial isolates associated with UTI was reported by employing aggregated citrate-reduced Ag NPs (Jarvis and Goodacre 2004). To acquire reproducible data, 50 spectra were collected making the spectral acquisition time ~8 min per bacterium. The multivariate statistical techniques were applied in order to group these organisms based on their spectral fingerprints. The results are shown in Fig. 6.8. The disadvantage was that all isolates were cultivated for 16 h and evidently more rapid analysis is required (Jarvis and Goodacre 2004). Recently, Premasiri and co-workers reported faster and direct analysis from urine samples obtained from patients (Premasiri et al. 2014). The sample preparation did not need any cultivation step. It was also easier in comparison to blood samples because the concentration of pathogen bacteria in urine is much higher than in blood and urine is a less complex body fluid than blood. Routine centrifugation and filtration led to 10^3–10^4 enrichment of bacterial concentration, which corresponds to clinically relevant concentrations and the typical threshold for antibiotic treatment. The SERS spectra of three different *Escherichia coli* strains that were spiked into urine at this minimal diagnostic level were analysed by SERS barcode procedure and PCA. After analysis, distinct clusters were obtained for the bacterial cells, demonstrating that specific spectral signatures can be identified. This test took about 40 min to perform thus it is very promising for rapid and low-cost UTI diagnosis.

7.3 SERS Cancer Diagnostics In Vitro

Reliable methods for cancer diagnosis and prognosis are a tremendous challenge for modern medicine. Detection of earlier stages of cancer is especially desirable because it reduces the risk of metastasis and gives a better chance for successful and efficient treatment. Owing to the progressive increase in human deaths resulting from cancer, a major effort is being made to develop noninvasive, effective and fast cancer detection. The sensitivity, speed and ease of use, together with strategies to achieve specificity make SERS an analytical approach that could be successful for real-time cancer diagnostics. It includes the SERS analysis of proteins, NAs, circulating tumour cells (CTCs), immunophenotyping of cancer cells as well as the detection of various tumour biomarkers such as cell surface markers or those produced by cancer cells.

There are potentially more than 150 biomarkers found in serum for the detection of various types of cancers. Examples are PSA or epidermal growth factor (EGF). Pancreatic cancer (PC) is one of the most lethal cancers and has a very poor prognosis because of the lack of a reliable tumour marker for early diagnosis. The most prevalent markers are mucin-type glycoproteins (MUC), which express elevated concentrations in PC patients. Mucins have emerged in recent years as useful markers for the early detection and predicting prognosis and response to therapy in several solid tumours because the expression of various mucin backbones and associated carbohydrate epitopes is altered during the initiation and progression of

various cancers, including PC. For most applications, single biomarkers are unlikely to provide the necessary sensitivity and specificity owing to the substantial heterogeneity among cancers. It is unrealistic to expect that a single biomarker will bring information about tissue type and malignant transformation throughout the various stages of tumour development and progression. Therefore, panels of biomarkers are needed, but before such panels can be employed in clinical practice, each biomarker must be discovered and validated individually (Phan et al. 2009).

7.3.1 Cancer Diagnostics Using NA Hybridization

The cancer susceptibility genes in DNA are associated with genetically predisposed cancer development. They can be detected in DNA isolated from patient's cells through SERS hybridization assays using labels. In the first model experiment of Allain and Vo-Dinh, the breast cancer susceptibility genes *BRCA1* nucleotide capture sequence (23-mer) labelled with rhodamine B was detected (Allain and Vo-Dinh 2002). Ag islands serving as SERS-active substrate were etched to form a microwell platform and subsequently modified with a monolayer of mercaptoundecanoic acid. The complementary probe was covalently bound to the Ag surfaces using a succinimidylester intermediate. In a hybridization experiment, the Ag surface coated with the immobilized capture oligonucleotides was used and the SERS spectra of the blank and the hybridized DNA were collected (Allain and Vo-Dinh 2002). Later, the hybridization probe was employed to oligonucleotides fragments labelled with cresyl fast violet containing a breast cancer sequence (Pal et al. 2006). The detection of a DNA sequence of the *Ki-67* gene, a critical breast cancer biomarker, on the triangular-shaped NWs substrate demonstrated the potential of the MS strategy for SERS-based DNA detection (Wang and Vo-Dinh 2009). Here, 150 μl of sample was spread over the entire chip area of 1.5 × 1.5 cm^2. SERS signal was acquired only from 15 pl fraction of the sample, which corresponds to 15 aM. For practical clinical applications, it would be desirable to have detection sensitivity in the range of 0.5–1.5 aM. Therefore, for clinical utilization, the authors stress the necessity of improving the sensitivity of the MS by an order of 10–30 times by the optimization of several fabrication parameters, such as probe surface density and chip size (Wang and Vo-Dinh 2009). DNA sensing using MS was further refined by development of a repeatable and reproducible MS-on-a-chip platform formed by triangular-shaped nanowire arrays having controlled gap (<10 nm) nanostructures over an entire 6 inch wafer (Wang et al. 2013b). Sun and co-workers designed the hybridization approach with the sensitivity close to 1 fM by using the Au NPs. The assay was able to detect alternative sequences in the gene splicing profile of the *BRCA1* gene linked to the malignant transformation of tumours in breast cancer (Sun et al. 2008). Later, the same group reported an advanced gene expression assay for *BRCA1* gene. It involved the isolation of RNA from breast cancer cell lines followed by a translation into complementary DNA

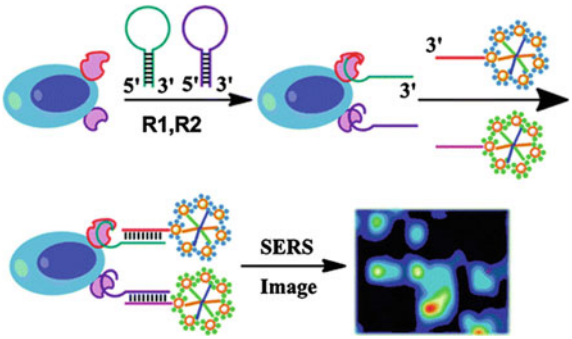

Fig. 7.7 Schematic diagram for simultaneous detection of two biomarkers on the cancer cell surface based on self-assembly of branched DNA–Au nanoaggregates (adapted with permission from Li et al. 2014. Copyright 2014 The Royal Society of Chemistry)

and sensitive quantification of the expression levels of splice junction, skipping exon 9 and 10, of the *BRCA1* gene (Sun and Irudayaraj 2009).

Recently, Li and co-workers applied aptamer-based recognition for simultaneous detection and imaging of two human breast cancer biomarkers MUC1 and nucleolin overexpressed on the MCF-7 cell surface (Li et al. 2014). The scheme of this experiment is shown in Fig. 7.7. Two hairpin-structured recognition probes (R1 and R2) composed of a target-specific aptamer sequence at the 5'-terminus and a linker segment at the 3′-terminus for connecting with the Raman probe. In the presence of target cancer cells, the aptamer can specifically recognize the biomarkers on the cell surface and undergo a conformational alteration, leading to stem separation. Following this, the (Au aggregates)/DNA hybridized with the opened stem and served as Raman probes for SERS measurement and imaging. To prepare the Raman probe, the hairpin DNA and barcode DNA modified by Raman dye label were simultaneously immobilized on the surface of Au NPs to form hairpin DNA-barcode-Au nanoaggregates, in which each Au NP can be loaded with a large number of Raman dye molecules. This proposed method possesses several advantages. First, by using DNA-gold nanoaggregates as Raman probes, the SERS signal can be significantly enhanced and the distribution of biomarkers can be readily visualized by SERS imaging. Second, this method permits simultaneous determination of two or more biomarkers on the cell surface. Third, as the aptamer sequence in the recognition probe can be easily replaced by other aptamers, the design can be conveniently used for detection of diverse ranges of biological targets.

Cancer diagnostics often needs a discrimination of genomic mutations in DNA sequences or special NA structures (miRNA) which can cause various diseases including cancer. SERS technique is very promising for mutation and single nucleotide polymorphisms detection because of the possibility of spatial multiplexing at array format linked with a portable biosensor device. Mahajan and co-workers reported such SERS-based approach using Au substrates prepared by

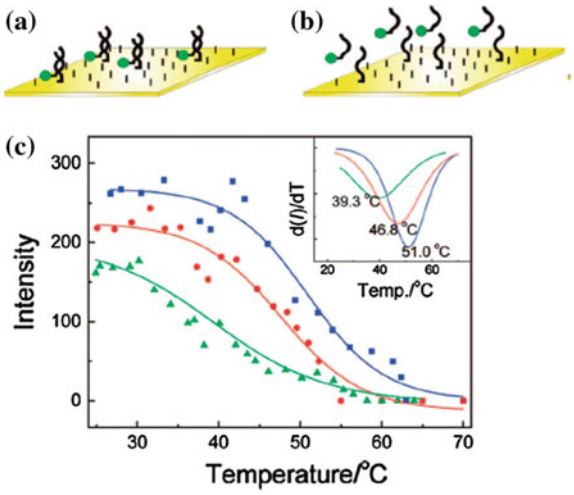

Fig. 7.8 SERS-based approach for discriminating mutations in DNA. **a** Labelled target sequences hybridized to capture oligonucleotides immobilized on the sphere segment void Au surface (label is marked by *green*). **c** Melting curves obtained from thermally induced dehybridization (**b**) of three different target sequences wild type without mutation (*squares*, *blue curve*), single point mutant (*circles*, *red curve*) and triple mutant (*triangles*, *green curve*). The first derivatives of the sigmoidal fits of the intensity curves are shown in the *inset* (adapted with permission from Mahajan et al. 2008. Copyright 2008 American Chemical Society)

electrodeposition around a close packed monolayer template (Mahajan et al. 2008). Their experiment is illustrated in Fig. 7.8. Disulphide-modified oligonucleotides were first immobilized on the sphere segment void Au surface to capture the corresponding target strand. Second, the Au surface was incubated with MH so as to cover the rest of the surface and thus avoid nonspecific binding. The target sequences were labelled with SERRS-active label and hybridized to the capture strand. SERRS label should be located near the Au surface to obtain a strong SERRS signal (Fig. 7.8a). Temperature and potential ramp were applied to the surface to obtain melting curves (Fig. 7.8b). The melting curves as a result of thermally induced dehybridization are shown in Fig. 7.8c. The SERRS intensity of the label was plotted against temperature for three different target sequences: wild type (no mutation), single point mutant and triple mutant (triple deletion). The wild type displayed the highest melting temperature (51 °C). It is because the target sequence matched perfectly the capture sequence. The melting temperatures of the single point mutant and the triple mutant were lower (46.8 and 39.3 °C, respectively) indicating a worse fit because of the mutation (Mahajan et al. 2008). In other experiment, the MS was applied to detect the single nucleotide polymorphisms at codon 504 of the *BRCA1* gene (Wabuyele et al. 2010). Hybridization with target DNA opened the hairpin and physically separated the Raman label (5-carboxy-tetramethylrhodamine) from the metallic NP. This reduced the plasmonic effect and quenched the SERS signal of the label. A linear relationship was

observed over low concentrations of target DNA (0–2 μmol l^{-1}) and reproducibility for the assay was <2 %.

Driskell and Tripp reported a label-free SERS detection of miRNAs based on affinity for an unmodified Ag NR array substrate (Driskell and Tripp 2010). MiRNAs are small noncoding RNA molecules that regulate eukaryotic gene expression and can serve as biomarkers of human cancers. The applicability of SERS for miRNA analysis was demonstrated using Ag NRs and the pathogenic relevant human miRNAs. The results indicated that miRNA sequences could be accurately discriminated and quantified even in multicomponent mixtures (Driskell and Tripp 2010). Later, highly reproducible Ag NRs were used to obtain SERS spectra of clinically relevant miRNA sequence in hybridization event. Straightforward LS analysis applied on SERS spectra enabled SERS quantitative determination of the relative ratios of the four nucleotide components: adenine, cytosine, guanine and thymine/uracyl (Abell et al. 2012).

7.3.2 Cancer Diagnostics Using Immunoassays

Sandwich immunoassays (described in Sect. 5.3.3) allowing specific detection of protein biomarkers are routinely used in clinical cancer diagnostics. Porter and co-workers developed immunoassays for SERS detection of PSA (Grubisha et al. 2003; Park et al. 2006; Porter et al. 2008). The assay for measuring PSA in human serum comprised a bifurcated fibre optical bundle for coupling the laser source to the Raman probe head, which focused the light onto the sample area and from the probe head to the Raman spectrometer. DSNB already activated for subsequent bioconjugation served as a RRM. DSNB was synthesized from the corresponding biscarboxylic acid using standard N-hydroxysuccinimide ester chemistry. The addition of DSNB disulfide to the Au NPs (32 nm diameter) led to the formation of a SAM monolayer on the metal surface. The DSNB ester terminus could subsequently react with the antibody by forming the corresponding amide. Such immunoassays showed LOD of PSA in human serum about 1 pg ml^{-1} (30 fM) with variation of signal less than 10 % from a different spot of the sample. It is necessary to mention that conventional assays have LOD of PSA about 100 pg ml^{-1} or above (Ferguson et al. 1996). The detection of PSA at a concentration 10 pg ml^{-1} and less helps patient relapse to be noticed months or even years quicker.

A SERS sandwich immunoassay has been applied successfully for quantitative measurements of MUC4 levels in the serum of patients with PC (Wang et al. 2011b). First, an Au-coated glass slide was functionalized with capture antibody through coupling with dithiobis-(succinimidyl propionate) ligands on the Au surface. Second, SERS tag was formed by a mixed thiol monolayer composed of dithiobis-(succinimidylpropionate) and RRM (4-NBT) on Au NP, followed by conjugation with the detection 8G7 antibody (Fig. 7.9a). This assay used the same anti-MUC4 antibody (8G7) for both capture and detection since it targets repeating epitopes (part of the antigen that is recognized by the antibody) of the MUC4

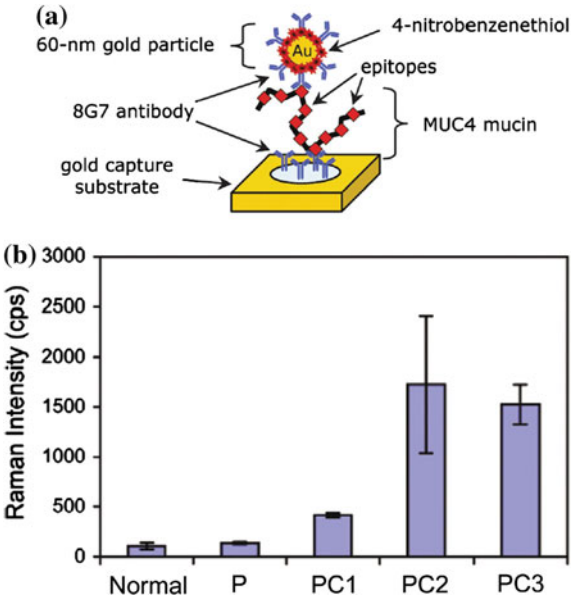

Fig. 7.9 Detection of MUC4 biomarker of pancreatic cancer using a SERS tag. **a** A schematic representation of the detection array. **b** SERS detection of MUC4 in pooled sera from normal individuals and patients with pancreatitis (P) or pancreatic cancer (PC1, PC2 and PC3). Each pool includes sera from 10 individuals (adapted with permission from Wang et al. 2011b. Copyright 2011 American Chemical Society)

molecules. In a typical immunoassay experiment, capture substrate was exposed to the sample solution for 8 h in a humidity chamber. After rinsing with buffer, captured MUC4 antigens were labelled by exposition to the functionalized NPs for 16 h. The substrates were then rinsed and dried with a stream of nitrogen and analysed by SERS. Concentration-dependent assay for MUC4 in the PBS buffer was performed. The analyte concentration was quantified using the peak intensity of 4-NBT at $\sim$1336 cm^{-1}. Based on these results, the SERS-based assay was applied to detect MUC4 in the serum of PC patients. Five sets of pooled serum samples were analysed after a 20× dilution in PBS: one pool from healthy individuals (normal), one pool from patients with acute pancreatitis (P) and three pools from PC patients (PC1, PC2, PC3). The results show that sera of patients with PC produce significantly higher SERS response for MUC4 compared to sera from healthy subjects (Fig. 7.9b). Later, they refined their diagnosis by using two relevant and well established markers for PC: serum carbohydrate antigen 19-9 (CA 19-9) and matrix metalloproteinase-7 (MMP-7). The LODs using the SERS platform were determined to be 2.28 pg ml^{-1} (matrix metalloproteinase-7) and 34.5 pg ml^{-1} (carbohydrate antigen 19-9) from spiked serum which is 29× and 14× lower for carbohydrate antigen 19-9 and matrix metalloproteinase-7 in comparison to ELISA technique, respectively (Granger et al. 2013). A novel SERS-based sandwich immunoassay using DNA aptamers, silica-encapsulated hollow gold nanospheres and a gold-patterned microarray was developed for sensitive detection of vascular EGF angiogenesis protein markers (Ko et al. 2013). Target specific DNA aptamers that fold into a G-quadruplex structure were used as a target recognition

unit instead of vascular EGF antibodies. The detection sensitivity was improved by 2 or 3 orders of magnitude over the conventional ELISA method.

The antibody-based recognition of two important cancer biomarkers, CEA and AFP, has been reported. In this experiment, a duplex SERS tag was created by coupling two antibodies against the cancer biomarkers on magnetic beads and both biomarkers were detected simultaneously in blood serum using a single excitation wavelength (Chon et al. 2011). Au patterned microarray was used as a matrix for the immuno-based detection of angiogenin which has an important role in tumour angiogenesis (Lee et al. 2011a). Park and co-workers reported the identification of HER2-positive breast cancer cell lines using antibody-conjugated Au NRs (Park et al. 2009). The Epstein-Barr virus-associated expression of latent membrane protein 1, a tumour marker for nasopharyngeal carcinoma, was also detected (Chen et al. 2012d). Immunoassay consisted of Au/Ag core-shell NPs coated with antibody specific to latent membrane protein 1 and 4-MBA as a RRM. Latent membrane protein 1 was detected in paraffin-embedded nasopharyngeal carcinoma tissues of patients that were positive for Epstein-Barr virus and healthy volunteers. The authors reported excellent accuracy of SERS: 97.1 % of the cancer patients were tested positive for the virus encoded protein, whereas only 64.7 % of the protein was detectable when a conventional immunohistochemical staining technique was applied (Chen et al. 2012d). A human p65 tumour suppressor and the cyclin-dependent kinase inhibitor p21cip (both proteins which are presented in elevated concentration in tumour cells) were detected in a multiplex SERS immunoassay based on antibody-functionalized Au/Ag NRs (Wu et al. 2013).

It has been found that breast cancer cells expressing the CD44 antigen and not the CD24 antigen exhibited enhanced invasive properties. The two cell surface markers C24 and C44 were detected by SERS in three human breast cancer cell (MCF-7, MDA-MB-231, MDA-MB-468) populations (Lee et al. 2011b). Au NPs functionalized with antibodies specific to CD24 or CD44 and different DNA sequences were used to target these two surface markers. Au NPs conjugated with corresponding complementary DNA sequences and RRMs were employed to form a network structure around the pointer NPs that can be detected by SERS. Fixed cancer cells were first incubated with pointer NPs to localize the NPs at corresponding membrane marker sites due to the antibody-antigen recognition. Then, the NPs were added to form the hybridization network structure at the corresponding marker sites targeted by the pointer particles. SERS mapping of two different RRMs, 4-mercaptopyridine (characteristic peak at 1094 cm^{-1}) and 4,6-dimethyl-2-pyrimidinethiol (characteristic peak at 569 cm^{-1}), representing CD44 and CD24, respectively, was conducted to determine the distribution of corresponding surface markers on selected cancer cells. The results indicated that MDA-MB-231 cells express the CD44 antigen and not the CD24 antigen (Lee et al. 2011b). Similarly, the selective targeting of chronic lymphocytic leukaemia was done using Ag NPs conjugated with anti-CD19 antibodies (MacLaughlin et al. 2013).

7.3.3 Direct Cancer Diagnostics from Blood Plasma

7.3.3.1 Cancer Diagnostics from SERS Spectra of Blood Samples

The direct SERS cancer diagnostics using blood plasma was discovered by the Chen group (Chen et al. 2012a). The procedure involved a mixing of crude blood or pretreated/purified blood samples with hydroxylamine-reduced Ag NPs, followed by SERS measurement and spectral analysis. Since the SERS from Ag NPs was often not reproducible, a drop of (Ag NP)/blood mixture was transferred onto an aluminium plate and SERS spectra were acquired using a confocal Raman microspectrometer. For each sample, three spectra were collected from different spot within the sample to obtain a mean spectrum. All these steps were completed within less than 3 h after the blood was drawn. SERS spectra were treated by PCA algorithms. It was found that, a combination of PCA and linear discriminate analysis (LDA) provided the best results. PCA was used for simplifying complex data sets and determining the key principal components in multidimensional data sets that best explained the spectral differences. LDA generated a diagnostic algorithm using the PC scores for the most significant PCs (Chen et al. 2012a). For example, the integration of the SERS spectral bands (at 1310–1430 and 1560–1700 cm^{-1} regions) achieved a sensitivity of only 70 and 83.3 % and a specificity of 76 and 78 %, respectively. However, the PCA-LDA algorithms yielded a diagnostic sensitivity of 96.7 % and a specificity of 92 % for separating cervical cancerous samples from normal samples (Feng et al. 2013).

The first report on SERS analysis of blood plasma for cancer diagnostics was nasopharyngeal cancer detection with diagnostic sensitivity 90.7 %, specificity 100 % and accuracy 95.4 % on a set of 33 normal subject and 43 nasopharyngeal cancer patient blood plasma samples (Feng et al. 2010; Chen et al. 2012a). Another SERS cancer diagnostics using Ag NPs reported by the Chen group involved a cervical (Feng et al. 2013), colorectal (Lin et al. 2011a) and esophageal (Li et al. 2013) cancer. Figure 7.10a compares the mean SERS spectrum for the cervical cancer plasma samples (blue curve, n = 60) with that of the normal plasma (red curve, n = 50). The peak positions and tentative assignment of major vibrational bands observed in blood plasma samples are listed in Table 7.1. The intensities of SERS bands at 1445 and 1580 cm^{-1} assigned to the CH_2 bending mode of collagen or phospholipids and amino acid Phe, respectively, are lower in healthy plasma than in cancer plasma. On the other hand, a decrease of signal intensities of SERS bands of Arg (496 cm^{-1}), Tyr (638 cm^{-1}), serine (813 cm^{-1}), galactosamine (888 cm^{-1}) and mannose (1135 cm^{-1}), reflects a tumour's vigorous metabolism. The peak at $\sim$1338 cm^{-1} of CH vibration of NA bases exhibits higher signal in the cancer samples indicating that there is an increase in the relative amount of NAs in the blood of cancer patient. Therefore, an abnormal NA metabolism (observed as circulating plasma DNA) of cancer cells (Gormally et al. 2007) can be used as biomarker for monitoring cancer occurrence in blood plasma samples. These spectral changes are typical for blood samples from all types of cancer patients

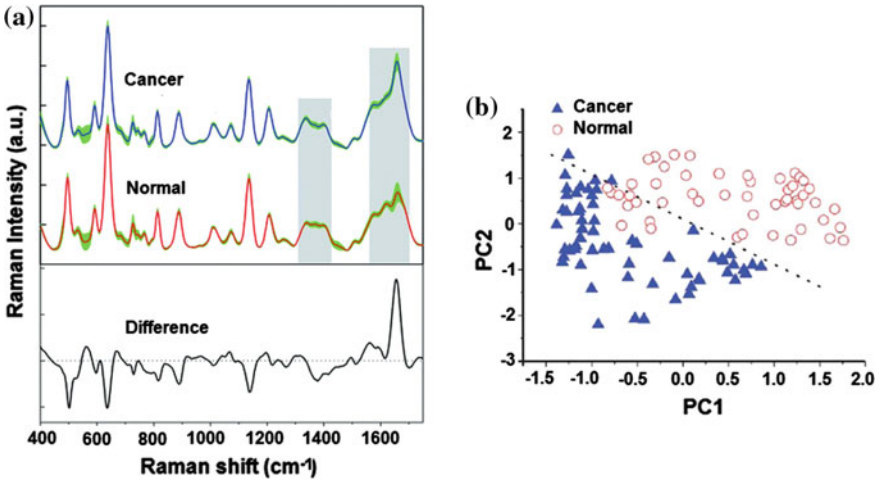

Fig. 7.10 Cervical cancer SERS detection from blood plasma. **a** Comparison of the mean spectrum for the cervical cancer plasma samples (*blue curve*, n = 60) versus that of the normal plasma (*red curve*, n = 50) samples. The *green shaded* areas represent the standard deviations of the means. *Black bottom* spectrum is the difference spectrum. **b** Plot of the first principal component (PC1) versus the second principal component (PC2) for the normal group versus the cervical cancer group. The *dotted line* as a diagnostic algorithm separates the two groups (adapted with permission from Feng et al. 2013. Copyright 2013 The Royal Society of Chemistry)

Table 7.1 The peak positions and tentative assignment of major vibrational bands observed in blood plasma samples, ν—stretching mode, δ—bending mode

Peak position (cm^{-1})	Vibrational mode	Major assignment
496	ν(S–S)	L-Arg
534		Cholesterol ester
638	ν(C–S)	Tyr
813	ν(C–C–O)	L-Serine
888	δ(C–O–H)	D-Galactosamine
1135	ν(C–N)	D-Mannose
1338		Adenine
1400	$\delta(CH_2)$	Collagen, phospholipids
1578	δ(C=C)	Phe
1655	ν(C=O)	Amide I

Reproduced with permission from Feng et al. 2013. Copyright 2013 The Royal Society of Chemistry

investigated up to now. PCA analysis showed that normal and cancer groups can be clearly separated (Fig. 7.10b).

Although the first results obtained for nasopharyngeal (Feng et al. 2010) and gastric (Feng et al. 2011) cancer were very promising, in both cases, the data points

for the normal as well as cancer patients were slightly overlapped preventing a clear separation of the two groups. To further improve the cancer detection using blood plasma, the Chen group introduced pretreatment and purification of blood plasma samples before SERS analysis (Lin et al. 2011b; Chen et al. 2012a). First, the purified plasma proteins (albumin and globulin) were separated from blood plasma by membrane electrophoresis, eluted and mixed with Ag NPs. Second, the SERS spectra were measured and analysed by PCA-LDA. Using these steps, the interferences of other native plasma constituents and exogenous substances were minimized and reliable spectral signatures were obtained. Thus, the gastric cancer group (31 patients) and the normal group (33 healthy volunteers) were completely discriminated with both diagnostic sensitivity and specificity of 100 % (Lin et al. 2011b; Chen et al. 2012a).

Recently, it was found that cancer can be detected by changes of molecular compositions and structures of human OxyHb (the common type of haemoglobin) in blood. SERS monitoring of such changes was applied to liver cancer investigations and diagnostic sensitivity 95.0 % and specificity of 85.7 % were achieved (Liu et al. 2013a). To improve reproducibility, Liu and co-workers developed Ag nanofilms from polyvinylalcohol-protected Ag NPs by electrostatic SAMs to obtain highly reproducible SERS spectra of human serum from 20 healthy donors. The major spectral features were reproducible but some spectral differences have been seen among spectra reflecting the diversity of the individuals (Liu et al. 2011). Later, a label-free serum RNA analysis enabled the detection of colorectal cancer by using 3D Ag nanofilm as a SERS-active substrate with sensitivity of 89 % and a specificity of 95.6 % (Chen et al. 2012b).

7.3.3.2 Detection of CTCs

Malignant cells are disseminating from a solid tumour and circulate in the bloodstream of patients manifesting a metastasis. The detection/identification of CTCs is therefore a promising cancer diagnostic approach. However, direct identification of CTCs is difficult since their concentration in blood is very low (only 1–10^3 CTCs per ml) compared to blood cells (10^9 per ml). Both capture sensitivity and specificity are critical for the detection of CTCs. SERS tags can be used to identify cancer cells in biological samples via specific membrane cancer marker binding.

SERS was successfully applied for the detection of CTCs in human blood. Sha and co-workers employed commercial SERS tags (Nanoplex biotags, Oxonica Inc.) comprised one or more Au NPs with a submonolayer of RRMs and protective silica coating (Sha et al. 2008). Magnetic beads functionalized with anti-epithelial cell adhesion molecule (EpCAM) antibodies immobilized on the surface served to capture of breast cancer SK-BR-3 cells spiked in human blood. Subsequently, the captured EpCAM-overexpressing cancer cells were detected with SERS tags. Scheme of the immunocomplex formed by SERS tag and magnetic bead conjugates

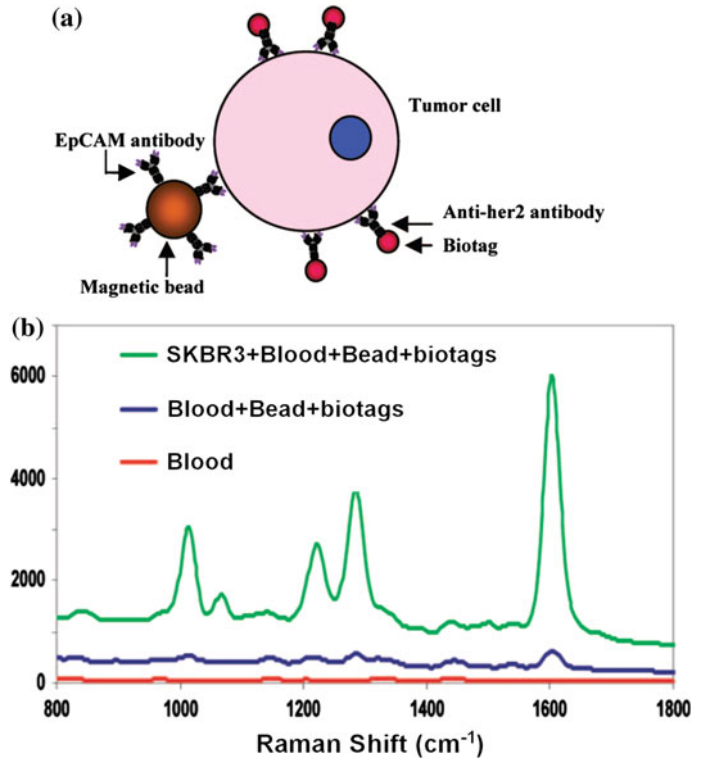

Fig. 7.11 Direct SERS detection of CTCs in blood. **a** Scheme of immunocomplex formed by Nanoplex biotags and magnetic bead conjugates binding to the model tumour cell. **b** Detection of breast cancer SK-BR-3 cells spiked into whole blood. SERS spectra of whole blood and of beads and biotag reagents in blood without and with SK-BR-3 cells spike (adapted with permission from Sha et al. 2008. Copyright 2008 American Chemical Society)

binding to the model tumour cell is illustrated in Fig. 7.11a. In contrast to other optical detection methods, near-IR excitation permitted the use of SERS tags in biological matrices such as whole blood. SK-BR-3 cells were spiked directly into whole blood prior to a short incubation of 30 min with magnetic bead-EpCAM and SERS tag-her2 conjugates. A magnet served to concentrate the magnetic beads along with captured cells to a specific position on the side of the tube where the SERS signal was collected. The results are shown in Fig. 7.11b. No SERS signal was detected from whole blood. In the absence of SK-BR-3 cells, a low background signal was observed when magnetic beads and SERS tags were added to whole blood. However, a strong SERS signal was detected when SK-BR-3 cells were spiked into whole blood, indicating that a signal can be directly acquired in whole blood without washing or additional handling steps. The detection limit was less

than 10 cells per ml with 99.7 % confidence in buffer solution. For the blood test, the cancer cells were spiked directly into whole blood prior to the incubation with capture particles and SERS labels. After magnetic enrichment, the SERS signal was obtained directly in whole blood without washing or other handling steps. The LOD in blood was about 50 cells per ml. This sensitive, simple and rapid assay platform requires no sample preparation and thus is promising for rapid clinical diagnosis and even real-time monitoring of the therapy progress.

Wang and co-workers successfully identified CTCs in the peripheral blood from patients with squamous cell carcinoma of the head and neck (Wang et al. 2011c). They employed Au NPs with RRM and functionalized with thiolated PEG layer to stabilize the NPs and minimize nonspecific interaction with blood cells. 15 % of PEG molecules have carboxyl functional groups for conjugation with N-terminus of EGF peptide. Detection limit was in the range of 5–50 tumour cells per ml of blood (Wang et al. 2011c). To achieve detection of CTCs with higher sensitivity and specificity, Shi and co-workers proposed a combination of magnetic enrichment and multiplex detection of CTCs by using targeted MNPs and SERS tags (Shi et al. 2014). SERS commercial tags (S440 and S420, Oxonica Materials Inc.) composed of a Au core (60 nm diameter) and a RRM adsorbed onto it. The NPs were conjugated with folate to target folate receptors of cancer cells. Both Au NPs and MNPs were targeted to folate receptor overexpressed on many cancer cells but absent on most normal blood cells. The results showed that only cells targeted with both SERS NPs and MNPs exhibit an increasing SERS signal due to magnetic accumulation of CTCs. Thus, the SERS signal increase correlates with CTCs detection. Free NPs or CTCs targeted with only SERS NPs or only MNPs did not exhibit this optical increase. The authors demonstrated SERS imaging system with 1 pM sensitivity and 2.5 mm penetration depth. A magnetic trapping system was able to effectively trap cells at flow velocities ranging from 0.2 to 12 cm s^{-1}. In addition, discrete SERS signals were detected in the magnetic trapping zone from a mixture of flowing dual-NP labelled HeLa cells and PBS buffer or rat blood indicative of single cell trapping events. Recently, Nima and co-workers presented a scheme for the multiplex detection of CTCs in whole human blood using tunable, silver-decorated, Au NRs as SERS multispectral contrast agents (Nima et al. 2014). Au NRs were functionalized with four RRMs and four antibodies breast cancer markers–anti-EpCAM, anti-IGF-1, receptor β, anti-CD44, anti-Keratin18, as well as leukocyte-specific marker anti-CD45. More than two orders of magnitude of SERS signal enhancement was observed from these hybrid nanosystems compared to conventional Au NRs.

7.3.4 Direct Cancer Diagnostics from Urine and Saliva

Recently, the Chen group presented a simple and noninvasive SERS diagnostics of cancer from urine and saliva using hydroxylamine-reduced Ag NPs (Huang et al. 2014; Feng et al. 2015). First, the impurities in the urine and saliva were removed

by centrifugation and the samples were then frozen to avoid degradation. In the case of saliva, the proteins were separated from saliva by membrane purification. Second, the samples were mixed with the Ag NPs and deposited on a piece of a rectangular aluminium plate. Urine SERS spectra were measured on esophagus cancer patients (n = 56) and healthy volunteers (n = 36) for control analysis (Huang et al. 2014). The prominent urine SERS peaks located at around 527, 656, 725, 807, 889, 959, 1002, 1138, 1209, 1342, 1376, 1465 and 1597 cm^{-1} can be visually observed in both normal and cancer urine, with the strongest signals at 725, 889, 1002 and 1138 cm^{-1}. A comparison of SERS spectra of the cancer urine with respect to the normal urine revealed a remarkable difference in spectral intensities: the normalized intensities of SERS peaks at 725 and 1465 cm^{-1} were higher for cancer than for healthy urine. Moreover, SERS peaks at 527, 889, 1002 and 1138 cm^{-1} were less intense for cancer than for healthy urine samples. These spectral differences were assigned to decrease in the relative content of urea and an increase in the percentage of uric acid in the urine of esophagus cancer patients compared to that of healthy subjects. The diagnostic algorithms utilizing a PCA-LDA method achieved a diagnostic sensitivity of 89.3 % and specificity of 83.3 % for separating esophagus cancer samples from normal urine samples.

Later, the saliva samples were used to demonstrate a capability for detecting benign and malignant breast tumours (Feng et al. 2015). A total of 97 SERS spectra from purified saliva proteins were acquired from samples obtained from three groups: 33 healthy subjects, 33 patients with benign breast tumours and 31 patients with malignant breast tumours. Comparison of the SERS intensities of the six prominent SERS peaks of saliva proteins (1004, 1049, 1176, 1265, 1340 and 1684 cm^{-1}) indicated significant differences between normal and breast tumour saliva samples. In contrast to the normal saliva protein samples, the benign and malignant breast tumour saliva proteins exhibited lower intensities at 1049 and 1176 cm^{-1}, but they showed much increased SERS signals at 1004, 1340 and 1684 cm^{-1}. In addition, the unusual SERS intensities associated with the different degrees of diagnostic utility were applied for discriminating between the three saliva protein groups (normal, benign breast tumour and malignant breast tumour). In particular, the malignant breast tumour samples showed greater intensities of SERS peaks at 1265 and 1684 cm^{-1} and much decreased signals at 1004, 1176 and 1340 cm^{-1} when compared with benign breast tumour saliva proteins. Multiclass partial LS discriminant analysis was utilized to analyse and classify the saliva protein SERS spectra from healthy subjects, benign breast tumour patients and malignant breast tumour patients, yielding diagnostic sensitivities of 75.75, 72.73 and 74.19 %, as well as specificities of 93.75, 81.25 and 86.36 %, respectively. These results demonstrated that saliva protein SERS analysis combined with discriminant analysis has good potential for the noninvasive and label-free detection of breast cancer.

7.4 SERS In Vitro Diagnostics of Other Diseases

In addition to pathogen's sensing and cancer diagnostics, SERS was applied to diagnostics of other diseases. This paragraph will introduce some examples.

The blood serum from type II diabetes, diabetics with complication and healthy volunteers was analysed by SERS (Han et al. 2009). The PCA successfully separated the diabetic patients from healthy volunteers with a sensitivity of 95 %, however, type II diabetes and diabetic complication groups were undistinguishable (Han et al. 2009). Recently, the Chen group first employed SERS to detect OxyHb variation in type II diabetic development (Lin et al. 2014). Label-free SERS spectra obtained from blood samples of 49 diabetic patients and 40 healthy volunteers using Ag NPs are compared in Fig. 7.12a. Differences in normalized spectral intensity between diabetic and normal OxyHb are clearly shown in their corresponding difference spectrum (bottom in Fig. 7.12b). The most obvious spectral differences (intensities and positions) can be found in the peaks at 478, 1212, 1312,

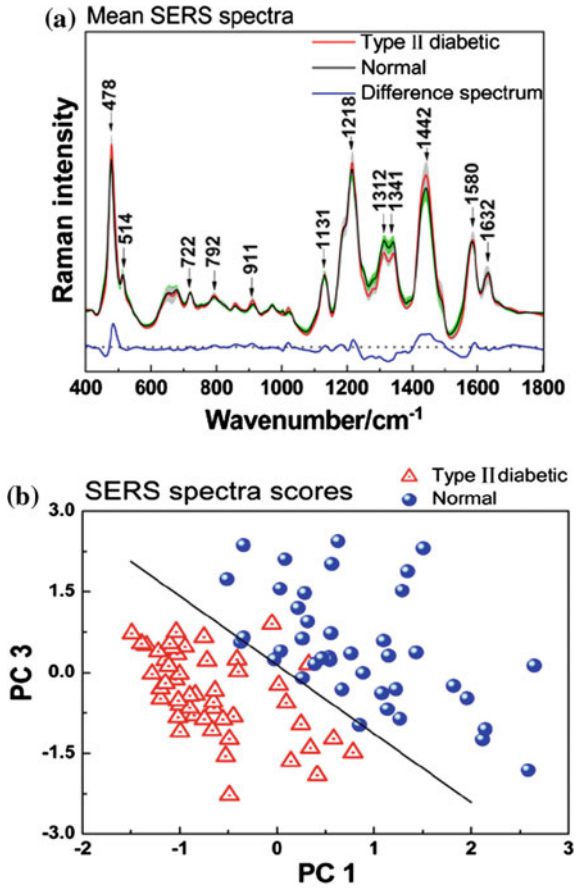

Fig. 7.12 Label-free SERS detection of type II diabetes. **a** Comparison of the mean SERS spectra of normal (*black line*, n = 40) and type II diabetic OxyHb (*red line*, n = 49). The *shaded areas* indicate the respective standard deviations. *Blue* spectrum is the difference spectrum. **b** Scatter plots of the PCA scores from the first principal component (PC1) and the third principal component (PC3) for the normal group (*blue circle*) versus the diabetic group (*red triangle*) (reproduced with permission from Lin et al. 2014. Copyright 2014 John Wiley & Sons, Ltd)

1341 and 1442 cm^{-1}. These changes were assigned to specific structural changes of OxyHb molecule in diabetes, including haem transformation and globin variation. To use OxyHb SERS spectra for discriminating diabetic from healthy patients, multivariate statistical methods based on PCA-LDA were performed on the measured SERS spectra. Scatter plots of the PCA scores from the first principal component (PC1) and the third principal component (PC3) for the normal group (blue circle) versus the diabetic group (red triangle) are shown in Fig. 7.12b. The solid line as a diagnostic algorithm by LDA separates the two groups with a sensitivity of 95.9 % (47/49), a specificity of 95.0 % (38/40) and an accuracy of 95.5 % (85/89).

In recent years, the infertility rate in married couples has been as high as 10–15 %, with male infertility comprising the majority of cases. Routine semen analysis based on microscopy and specialized software programs includes examination of such sperm parameters as concentration, motility and vitality. However, this method is only approximative and subjective. It is known that semen consists of a cellular part and noncellular part. The noncellular part (seminal plasma) has been found to be related to spermatozoa (mature male germ cells) function. Analysis of seminal plasma can predict sperm quality and has the potential to assess male fertility. SERS analysis and differentiation of seminal plasma was for the first time reported (Chen et al. 2012c). In this work, 61 semen samples (24 normal and 37 abnormal) were used. The spermatozoa were removed from sperm samples by centrifugation to obtain the seminal plasma. A pipette tip was applied to create a mixture containing the seminal plasma and the hydroxylamine-reduced Ag NPs in 1:1 proportions. Then, the mixture was transferred to a rectangular aluminium plate for SERS measurements. For the normal and abnormal seminal plasma, the SERS peaks at 649, 720, 809, 954, 1132, 1220, 1445 and 1584 cm^{-1} can be clearly identified. However, the SERS peaks at 649, 720 and 954 and 1584 cm^{-1} were more intense in the normal group than those in abnormal group and the peaks at 809 and 1132 cm^{-1} were more intense in the abnormal group. Distinctive SERS features and intensity differences between normal and abnormal seminal plasma could reflect molecular changes associated with the process of sperm abnormality. For example, the band at 649 cm^{-1} was attributed to the guanine ring breathing mode indicating higher content of guanine in the normal group than in the abnormal group. The relative SERS peak intensity at 720 cm^{-1} due to coenzyme A was found to be lower in the abnormal group than in the normal group. The peak at 954 cm^{-1}, which can be attributed to the spermine phosphate hexahydrate, was more intense in the normal group than that in the abnormal group. The diagnostic performance in differentiating abnormal seminal plasma (n = 37) from normal seminal plasma (n = 24) was evaluated. A PCA-LDA analysis of results obtained for different laser polarizations demonstrated different diagnostic sensitivities and specificities, among which, left-handed circularly polarized laser excitation showed the best diagnostic result (95.8 % sensitivity and 64.9 % specificity).

Buoyant silica bubbles were employed as capture substrates in a cholera SERS immunoassay (Schmit et al. 2012). Silica bubbles were silanized and then functionalized with an anti-cholera toxin antibody. Au NPs were used as SERS

substrates. The freshly prepared NPs (50 nm diameter) were labelled with 1,2-bis (2-pyridyl)ethylene coated with a silica shell and then incubated with the anti-cholera toxin antibody solution to allow antibodies to adsorb on the silica-coated Au NPs. After that, recombinant β subunit cholera toxin antigen was incubated with the capture bubbles and functionalized Au NPs. Buoyancy could pull the immunocomplexes from the sample solution to a compact monolayer of bubbles on the surface of the sample. Following the incubation, the entire reaction suspension was transferred to a polished aluminium surface where the bubbles were allowed to rise to the surface for about 5 min. SERS was collected from the monolayer of the bubbles on top of the sample volume. The detection limit of this assay for the β subunit of the cholera toxin in a buffer was 1100 ng.

Chon and co-workers developed a fast and sensitive SERS-based competitive immunoassay using SERS tags and magnetic capture beads for the early diagnosis of acute myocardial infarction (Chon et al. 2014). In this novel assay technique, free target antigens and antigen-conjugated tags based on hollow gold nanospheres reacted competitively with monoclonal antibodies on magnetic capture beads. The simultaneous quantification of dual acute myocardial infarction biomarkers in patient serum, namely, cTnI and CK-MB, was successfully achieved within a single excitation wavelength. This SERS-based competitive immunoassay has multiple advantages including a quick assay time (less than 15 min), an easy assay procedure (using magnetic beads), small sample consumption (minimum of 10 ml) and simultaneous dual marker detection using reliable, sharp and easily distinguishable SERS peaks.

Many neurological diseases are caused by the aggregation of specific types of proteins inside and/or outside of cells causing a kind of fibrosis. Diseases such as Alzheimer's, Parkinson's, Creutzfeldt−Jakob's, Huntington's, as well as prion diseases and amyotrophic lateral sclerosis, are being diagnosed by identifying protein aggregation (Kopito 2000). β-amyloid peptide, which is a small molecule that forms brain plaques and Alzheimer's disease, has been detected and characterized using a nanofluidic SERS device (Chou et al. 2008; Choi et al. 2012). This nanofluidic device was fabricated from PDMS microchannels by using photolithography to create nanochannels. Parkinson's and Alzheimer's diseases are also characterized by a form of abnormal enzyme activity. In the study of Stevenson and co-workers, Au NPs were incorporated by cell populations along the colourless substrate, where upon internalisation it was enzymatically transformed by β-galactosidase enzymes to 5,5′-dibromo-4,4′-dichloroindigo (Stevenson et al. 2013). This transformation was characterized by the appearance of a peak in the SERS spectra at 598 cm^{-1} and a blue colour which was indicative of the turnover of the substrate by the enzyme. The conversion was specific to the enzyme as confirmed when known enzyme inhibitors were introduced and the corresponding reduction in the measured SERS signal was observed. High resolution analysis of single cells and cell populations suggested that enzyme action was localized in specific cellular compartments which were proposed to be endosomes. The authors expressed a desire to quantify enzyme levels within these compartments, particularly in

response to different disease stimuli and states (Stevenson et al. 2013). Recently, Guerrini and co-workers reported SERS platform for detection of amyloid oligomers on metallorganic-decorated plasmonic beads. Here, the detection is based on the sensing properties of hybrid Au-decorated PS beads that are engineered with an effective metallorganic Raman chemoreceptor, composed of Al^{3+} ions coordinated to 4-MBA (Guerrini et al. 2015). The thiol group of 4-MBA bound the Au surface via Au–S covalent bonds, whereas the carboxylic groups of 4-MBA chelated the Al^{3+} ions forming a coordination complex and offering effective adsorption sites for oligomer interaction. The SERS platform was tested on oligomers formed from the N-terminal domain of the *Escherichia coli* protein HypF. The 4-MBA-Al^{3+} chemoreceptor decorating Au-PS beads experienced mechanical deformations of its phenyl ring upon complexation with HypF-N oligomer species, which are registered in their SERS spectrum and served for their quantitative detection. The plot of the SERS intensity values versus oligomer concentration demonstrated a linear correlation ($r^2 > 0.98$) and LOD of 0.1 μM, which corresponded to less than 6 pmol in the analysed sample volume (60 μl).

A highly sensitive immunoassay in a microfluidic system for Hepatitis B virus antigen from human blood was developed (Kaminska et al. 2015). The Au nanoflowers labelled with fuchsin as RRM formed a sandwich structure with the antigen and the antibody immobilized on the Au/Ag coated GaN support served as SERS-active substrate. They showed that if the microchannels are fabricated by such support it provides more sensitivity in comparison to the microchannels made from PDMS. In clinical practice, the presence of Hepatitis B virus antigen is monitored in whole blood, serum or plasma. In this study, the authors demonstrated that their SERS-based immunoassay could be used for the detection of Hepatitis B virus antigen in human serum or plasma samples. Quantitative analysis was performed by plotting the SERS intensity of the fuchsin marker band at 1178 cm^{-1} versus the concentration of the antigen. The LOD for Hepatitis B virus antigen was estimated to be ~40 times lower than the LOD of the ELISA. RSD of this method was less than 10 %.

Lactic acid is a simple and effective indicator for estimating physiological functions. The normal physiological range is about 0.55–1.67 mM in clinical diagnostics. Lactate is an important indicator of potential mortality in intensive care patients. To demonstrate multianalyte sensing capabilities with partition layer-modified substrates, the Van Duyne group prepared Ag FONs with DT/MH mixed SAMs to detect both glucose and lactate (Shah et al. 2007). They reported quantitative analysis of lactate in the concentration range of 10–240 mg dl^{-1}. Sequential injection of lactate and glucose into a flow cell was used to demonstrate the capability of the sensor to discriminate between the two analytes. Hsu and Chiang applied Ag NPs for rapid and quantitative SERS detection of lactic acid in human serum. The sensitivity of detection is about 10^{-5} M at a 50 s acquisition time (Hsu and Chiang 2010).

Creatinine is an endogenous degradation product of muscle metabolism and its serum or urine concentration can be the primary indicator in establishing renal function. The SERS spectra of creatinine from human serum down to 0.1 μg ml^{-1}

concentration were obtained using Ag NPs within 200 s acquisition time (Stosch et al. 2005). (Ag NP)/(Graphene oxide) hybrid structures were employed to intrinsic detection of folic acid (vitamin B related to many diseases including heart attacks, congenital malformation and mental devolution) in serum (Ren et al. 2011). The modification of graphene oxide with positively charged poly(diallyldimethyl ammoniumchloride) was employed for the electrostatic self-assembly of the negatively charged Ag NPs onto graphene. The folic acid was bound to the positively charged hybrid surface via electrostatic interaction, which provided a SERS signal. The LOD for folic acid was 9 nM and the calibration curve showed a good linear relation in the concentration range from 9 to 180 nM.

7.5 SERS-Based Medical Therapy and Theranostics In Vitro

One of the efficient therapeutic procedures is a photodynamic therapy (PDT), which combines the use of light at appropriate wavelengths with a photoactive drug (photosensitizer) to produce highly toxic reactive oxygen species. Theranostics is a new technology, which combines diagnostics and therapy. Such a combination can increase the specificity and efficacy of therapeutics, resulting in improved outcomes and reduced side effects. SERS-based theranostics incorporates SERS as the diagnostic imaging modality, which offers easy multiplexing and does not suffer from photobleaching (Vo-Dinh et al. 2015). To achieve efficient cellular damage via PDT, it is necessary to deliver the appropriate light dose and photosensitizer concentration at the site of interest. In order to better understand drug delivery, precise observation of drug release and delivery is required. The analytical interest is related to detection and distribution of anticancer agents inside cancer cells and their cytotoxic activity after photothermal treatment. Anticancer agents are highly cytotoxic and thus cannot be accumulated in the cells at concentrations higher than nanomolar. Therefore, SERS because of its high sensitivity is a suitable technique for this purpose. The strong absorption and efficient heat conversion of metallic nanostructures suggest that they can be highly promising plasmonic photothermal therapeutic (PPTT) agents (Link and El-Sayed 2000). Metallic nanostructures, predominantly Au ones, in many different forms (i.e. NPs, NRs and nanostars), have been utilized for the destruction of cancerous cells. SERS macroscopic imaging can help to localize the nanostructures inside the cells.

Chourpa and co-workers recorded simultaneously the fluorescence emission and SERRS spectra of the anticancer drug mitoxantrone over the cell (Chourpa et al. 2008). The spectra confirmed the presence of small Ag NP aggregates when they contain fluorescence background superimposed with SERRS signal of mitoxantrone, noticeable due to the most intense band at $\sim 1300\ cm^{-1}$. A semiquantitative analysis of the intracellular spectra was used to deconvolute into a proportional addition of characteristic fluorescence and SERRS spectra. The deconvolution coefficients

served to generate specific fluorescence and SERRS maps that could be superimposed with the white light image of the cell. Analysis of such SERRS/fluorescence multispectral maps provided multiple information about the drug molecular contacts in a given subcellular compartment (Chourpa et al. 2008). Kang and co-workers presented SERS/fluorescence imaging spectroscopy approach to monitor in real-time the uptake and release of anticancer drug doxorubicin (DOX) from Au NPs at a single cell level (Kang et al. 2013). Their study is illustrated in Fig. 7.13. The DOX molecules were conjugated to Au NPs via a hydrazone linker, which is sensitive on local pH. Following PEGylation, arginylglycylaspartic and nuclear localizing signal peptides were conjugated to the NP surface to increase internalization of the Au NPs as well as selectively deliver it to the cell nucleus. When DOX

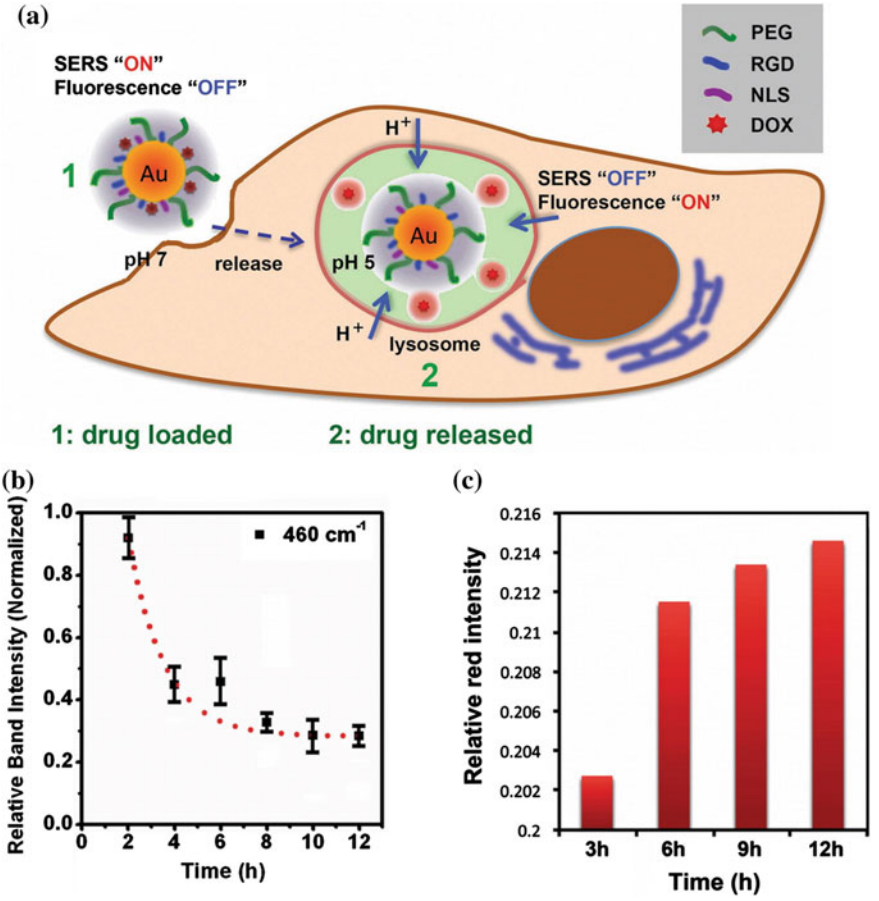

Fig. 7.13 pH-triggered DOX release tracking in acidic lysosomes. Schematic diagram of experiment (**a**), real-time monitoring of the DOX release from Au NPs in HSC-3 cells by SERS spectra (**b**) and fluorescence (**c**) (adapted with permission from Kang et al. 2013. Copyright 2013 The Royal Society of Chemistry)

was bound to the Au NPs, its SERS spectrum could be observed, while the fluorescence was quenched. When the DOX-loaded Au NPs were internalized by the cells, the hydrazone bond was cleaved at the acidic pH of the lysosomes causing the release of DOX molecules from Au NPs. Consequently, SERS signal of DOX significantly decreased and fluorescence of free DOX molecules appeared (Fig. 7.13a). In order to monitor the release dynamics of DOX in real-time, human oral squamous carcinoma (HSC-3) cells were incubated with DOX(0.2 nM)/(Au NP) and both Raman and fluorescence signals were recorded at different instants of drug treatment. The intensity of the 460 cm^{-1} DOX band was found to decrease continuously at 4 h of DOX/(Au NP) incubation until it completely disappeared after 12 h of treatment (Fig. 7.13b). Figure 7.13c shows the relative intensity of the DOX red fluorescence at different times. The red fluorescence intensity increased in cells over time indicating the continuous release of DOX molecules from Au NPs via hydrazone bond breakage induced by the slightly acidic pH microenvironment of the lysosomes (pH 5.0). Both SERS and fluorescence data indicated that the DOX release from the Au NPs was time-dependent.

Song and co-workers reported a theranostics strategy based on plasmonic vesicles assembled from Au NPs for targeted drug delivery, which can be tracked by SERS spectroscopy (Song et al. 2012). The SERS tag contains the RRM, mixed brushes of hydrophilic PEG and pH-sensitive hydrophobic copolymers of PMMA and 4-vinylpyridine to allow drug release, HER2 antibodies for cancer cell targeting and encapsulated DOX. To prove this concept, the study was performed with breast cancer cells overexpressing EGF receptor 2 (HER2). The vesicle-coated cancer cells displayed a strong SERS signal of the RRM that gradually decreased with time caused by acidic driven disruption of the vesicles and a drug release.

The release of a dye/drug from Au nanocages formed by Au nanocubes was also monitored by SERS (Tian et al. 2013). Nanocages with an edge length of $\sim$73 nm and wall thickness of $\sim$6 nm were produced by galvanic replacement of Ag nanocubes by Au. The surface of the Au NPs was first modified by PEG to improve the biostability and reduce nonspecific binding of proteins. Second, arginylglycylaspartic and nuclear localizing signal peptides were conjugated to the Au NP surface to increase their internalization as well as selectively deliver the Au NPs about the cell nucleus. Nile red and DOX were used as the model cargo and loaded into the nanocages together with 1-tetradecanol. Phase change of 1-tetradecanol can be controlled by a temperature, which can serve to ensure the release of the drug in response to an external stimulus. The phase change of 1-tetradecanol is used for encapsulating drugs at lower temperature. After the loading with drugs, SERS spectra were recorded from the plasmonically active nanocages. The encapsulated molecules can be released along with the melted 1-tetradecanol through diffusion after raising the local temperature by thermal or ultrasonic means. During the drug release experiment, the 785 nm laser induced photothermal effect led to melting of 1-tetradecanol and it resulted in the release of the drug from the nanocages. The release of nile red and DOX from the nanocages was monitored by SERS when

decrease of the SERS intensity with increasing laser exposure time was observed. Importantly, 1-tetradecanol has a melting point at 38–39 °C which is only slightly higher than the normal human body temperature.

Investigation of the molecular changes of cancer cells with drugs treatment is crucial for the design of new anticancer drugs and the development of novel diagnostic strategies. The local pH inside glioma U-87 MG cancer cells was monitored after PDT treatment by 6-methyl-1,3,8-trihydroxyanthraquinone (emodin) drug (Bálint et al. 2011). The cellular pH was determined by the real-time measurement of the SERS from a pH-sensitive probe 4-MBA that is embedded in the cell. The SERS tag was a micrometre-sized silica bead covered by nanosized Ag NPs with 4-MBA as RRM. Visible excitation at different light dosages was used to activate the drug. The results indicate cell maintenance of internal pH and cell death at low and high light dosage, respectively (Bálint et al. 2011). Recently, to analyse the detailed effects of targeting ligands on cell nuclei, in situ SERS detection was performed by the Raman platform with the assistance of dark-field and fluorescence microscopes to simultaneously locate Au NRs and small molecules (Liang et al. 2015). Here, human gastric carcinoma (SGC-7901) cell nuclei were treated with two model drugs, DNA binder (Hoechst33342) and DOX. Nuclear targeting nanoprobes with an assembly structure of thiol-modified PEG and nuclear localizing signal peptides around Au NRs were prepared to achieve the amplified SERS signals of biomolecules in the cell nuclei. Through the analysing of SERS spectra measured from the cell nucleus, they found that both drugs can cause the obvious changes of DNA and proteins.

The combination of SERS tag and PDT drug carrier into a single platform is also promising for theranostic applications. Lu and co-workers reported SERS monitoring of PDT on prostate cancer cells by using popcorn-like Au NPs (Lu et al. 2010). Spherical Au NPs were prepared by citrate-reduction and then ascorbic acid was added as a reducing agent in the presence of CTAB as a shape-templating surfactant and Au nanopopcorns were formed. For selective sensing, therapy and monitoring of therapy progress, Au nanopopcorn NPs were conjugated with multiple targets specific for membrane PSA: anti-PSA antibody and RH6G attached to A9 RNA anti-PSA aptamers. RH6G-modified RNA aptamers covalently attached to the surface have a dual function as targeting molecules and Raman dye-carrying vehicles. RH6G modification on the RNA aptamer was used as a RRM for SERS measurement. Photothermal treatment of the human prostate cancer (LNCaP) cells was performed with 785 nm laser radiation. SERS detection was carried out by using 670 nm excitation wavelength. The decrease of the SERS intensity was attributed to the breaking of the S–Au bond between the Au NPs and the RH6G-modified A9 RNA aptamer caused by the strong photothermal effect. This change was not observed when the target cells were absent: in this case no aggregates were formed and the LSPR at 580 nm could not be excited by the NIR laser radiation (Lu et al. 2010). Beqa and co-workers introduced an aptamer-conjugated hybrid nanomaterial (Au popcorn-like NPs attached to carbon nanotubes) as a probe for targeted diagnosis and PDT of human breast cancer cells (SK-BR-3), even at level of 10 cells per ml (Beqa et al. 2011). The results showed

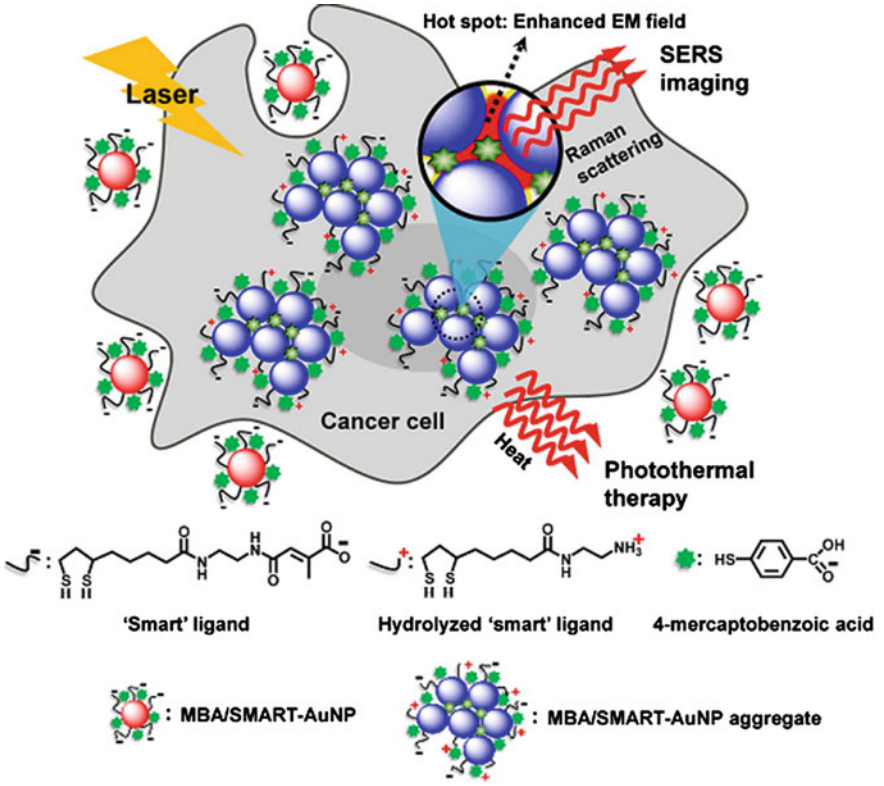

Fig. 7.14 Schematic illustration of the working mechanism of 4-MBA/(SMART-Au NPs) in a cancer cell. See text for details (reproduced with permission from Jung et al. 2013. Copyright 2013 American Chemical Society)

significant SERS enhancement with the addition of SK-BR-3 cells because the nanoprobes were highly specific to HER2, which promotes the growth of cancer cells. HER2 expressed in the SK-BR-3 breast cancer cells. This approach distinguishes between the different breast cancer cell lines.

Jung and co-workers prepared "SMART" Au NP tags for simultaneous Raman imaging/diagnosis and photothermal therapy (Jung et al. 2013). Schematic illustration of the working mechanism in a cancer cells is shown in Fig. 7.14. The "SMART" Au spherical NPs (10 nm diameter) were covered with surface molecules that contain hydrolysis-susceptible citraconic amide units ("smart" ligands) and pH sensitive RRM (4-MBA). The NP surfaces were engineered to have both positive and negative charges which induce rapid aggregation of the NPs by electrostatic interactions under mildly acidic conditions. Upon internalization by the cell, 4-MBA/(Au NPs) aggregated as the result of pH-sensitive surface charge on the NPs. The aggregates served as SERS imaging tags providing strong SERS signal due to the existence of "hot spots". The aggregation shifted the LSPR to the

NIR region due to the appearance of coupled plasmon modes. This shift was successively used for selective and deep-tissue-penetrating photothermal therapy. In therapeutical experiment, B16 F10 cancer (mouse melanoma) cells were coincubated with 4-MBA (40 nM)/(SMART-Au NPs) for 12 h. Control cells were prepared using 4-MBA (40 nM)/(Au NPs) without "smart" ligands or with no Au NPs. SERS spectra were acquired from the cells using a microscope system with 785 nm laser excitation. The 4-MBA/(SMART-Au NPs) sample showed the distinct SERS peaks, while the 4-MBA/(Au NPs) without "smart" ligands and no Au NP control samples showed no detectable signal. Representative spots in the 4-MBA/(SMART-Au NPs) sample and the control samples were irradiated for 10 min by the same 785 nm laser with a 19.5 W cm^{-2} power density. For the 4-MBA/(SMART-Au NPs) sample spots, distortion in the cellular morphology was observed which is indicative of the cell mortality. No noticeable changes were found for the control 4-MBA/(Au NPs) without "smart" ligands and no Au NP samples under identical laser irradiation. The experiment was repeated with higher NP concentration (100 nM) and longer incubation time (24 h). The theranostic Au NPs are cancer-specific because they aggregate rapidly and accumulate selectively in cancerous cells.

The Vo-Dinh group reported the combination of SERS detection and PDT in a silica-coated gold nanostars platform (Fales et al. 2011). The SERS tag was formed by Au nanostar labelled with a 3,3′-diethylthiatricarbocyanine (DTTC) as RRM. The Au nanostars have a higher plasmonic effect than Au spherical NPs under the red excitation conditions. DTTC has strong absorption in NIR region providing strong SERRS signal with 785 nm excitation. The silica shell of SERS tag was then loaded with a fluorescent PDT photosensitizer (MB) that could be activated at 633 nm. The 785 nm wavelength of light falls outside of the absorption band of MB, thus preventing any unwanted activation of the photosensitizer. Thus, SERRS detection could be performed at 785 nm and PDT at 633 nm, with no interference between the two modalities. Upon excitation at 785 nm, SERRS was observed from the NIR Raman dye on the nanostar surface. Excitation at 633 nm generated fluorescence (and singlet oxygen) from the MB. PDT on BT549 breast cancer cells after incubation with MB-loaded particles and light exposure was clearly observed. The same light exposure was performed on cells treated with silica-coated nanostars that did not contain MB, showing no evidence of any photothermal effects (Fales et al. 2011). The theranostic nanoplatform was further functionalized with a cell-penetrating peptide (TAT), which increased intracellular accumulation of SERS tags (Fales et al. 2013). In this case, the Au nanostars were labelled with a dye to match the 633 nm excitation and protoporphyrin IX was encapsulated in the silica shell as the PDT photosensitizer. After activation using UV light, the greater number of SERS tags per cell provided SERS spectra for Raman imaging and PDT effect. In contrast, without TAT, not enough SERS tags were delivered into the cells to allow Raman imaging (Fales et al. 2013). The limitation of this approach is the necessity of using two excitation wavelengths (one for SERS imaging and one for PDT) and the difficulty to discern the fate of two components (RRM and photosensitizer) in a biologically complex environment.

Recently, Farhadi and co-workers proposed a novel approach which enables obtaining the spectroscopic SERS information during light irradiation for PDT. Here, Pd-pyrolipid photosensitizers that are essentially not fluorescent were employed. Pd-pyrolipid theranostic NPs, when excited by same excitation wavelength (638 nm), simultaneously were both PDT active and emitted a strong SERS signal (Farhadi et al. 2015). A unique multifunctional theranostic SERS tags were developed with gold nanostars for SERS, magnetic resonance imaging (MRI), computed tomography (CT), two-photon luminescence (TPL) imaging and PPTT. The synthesized gold nanostars were tagged with a RRM (4-MBA) and linked with an MRI contrast agent Gd^{3+} (Liu et al. 2013b). These tags have LOD of 2 pM (SERS), 10 pM (MRI) and 100 pM (CT). Tumour phantom experiment demonstrated the potential of multifunctional nanoprobe for future in vivo applications. The photothermal ablation was performed under 850 nm excitation proved cell death following irradiation whereas cells in the area which was not irradiated remained alive.

Noh and co-workers employed Au/Ag hollow nanoshells (HNSs) and Au NRs as multifunctional therapeutic agents for effective, targeted, photothermally induced drug delivery under NIR light (Noh et al. 2015). Au/Ag HNSs and Au NRs showed similar photothermal efficiency under optimized NIR laser power. SERS tag was formed by PEGylated HNSs conjugated with antibodies against the EGF receptor (EGFR) and with the antitumour drug DOX for lung cancer treatment. The targeting of such SERS tag was confirmed by light scattering images of human lung carcinoma A549 cells and DOX release from the HNSs was evaluated under low pH and NIR-irradiated conditions. Multifunctional SERS tags induced photothermal ablation of the targeted lung cancer cells and rapid DOX release following irradiation with NIR laser. Furthermore, the authors evaluated the effectiveness of HNS/EGFR/DOX tags for drug delivery by comparing two drug delivery methods: receptor-mediated endocytosis and cell-surface targeting. Accumulation of the SERS tags on the cell surfaces by targeting EGFR turned out to be more effective for lung cancer treatments than its uptake. The results suggest a new and optimal method of NIR-induced drug release via the accumulation of targeted SERS tags on cancer cell membranes.

7.6 SERS Ex Vivo: Tissue Diagnostics and Histology

Detection and localization of prognostic markers in tissues were applied for cancer diagnostics. For example, PSA can be used for identification of tumours tissues from patients undergoing prostatectomy. In 2006, this approach was first reported by Schlücker and co-workers using SERS tags formed by Au/Ag nanoshells containing aromatic RRMs and a PSA antibody (Schlücker et al. 2006). SERS from the RRM was detected in the epithelium (PSA positive) of the incubated prostate tissue section. Stroma and lumen (PSA negative) locations served as controls.

Unique composite organic-inorganic NP (COIN) served as a part of SERS tags for PSA localization in the prostate tissue (Sun et al. 2007). COIN is a nanocluster formed by Ag NPs aggregated by organic analyte in the presence of an inorganic RRM. Ag COIN provides higher SERS enhancement and the possibility to use a broader range of RRMs in respect to gold. PSA in tissue samples from the human prostate was detected ex vivo using the Ag COINs encapsulated by BSA layer and functionalized with PSA antibodies (AbPSA). The schema of a direct binding assay is shown in Fig. 7.15a. Two different COINs, one conjugated with acridine orange and one conjugated with basic fuchsin as RRMs, were selected for multiplex tissue analysis. The major components of the SERS spectrum determined from LS analysis are signals from (basic fuchsin)/AbPSA (blue), (acridine orange)/AbPSA (red) and tissue autofluorescence (grey) (Fig. 7.15b). The best fit spectrum is indicated in black and the small error shown is typical of this kind of duplex

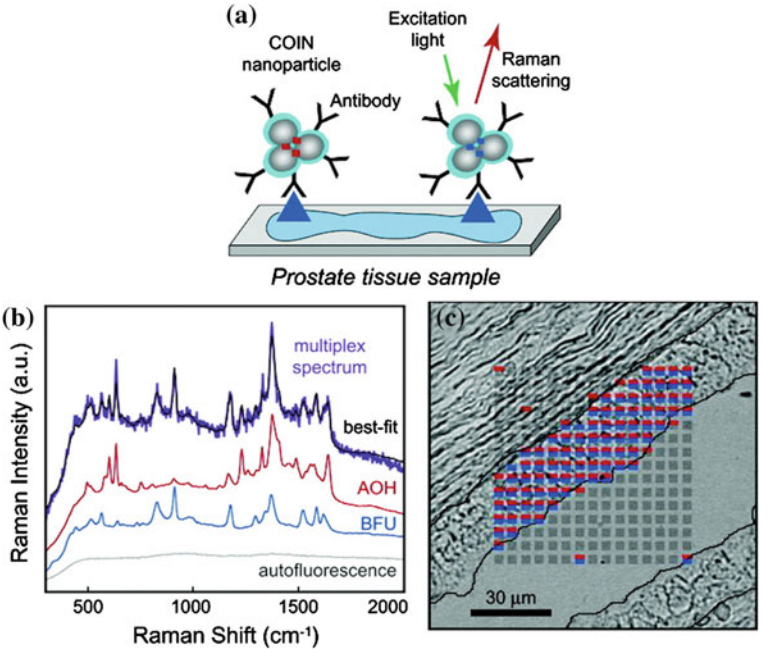

Fig. 7.15 Simultaneous two-COIN staining in the direct PSA detection assay in tissue. **a** Schematic representation of a direct binding assay. **b** Spectral fitting in duplex COIN experiments on tissue. The upper set of spectra are the measured spectrum from a single point in the epithelium (*purple*) and the best-fit spectrum (*black*) found from LS regression using reference spectra. The major fitting components are the two conjugated COINs: (acridine orange)/AbPSA (*red*), (basic fuchsin)/AbPSA (*blue*) and the tissue autofluorescence (*grey*). **c** PSA expression patterns reported by two COINs in a simultaneous duplex measurement. In each pixel, colour represents PSA-positive classification based on (basic fuchsin)/AbPSA (*blue*) and (acridine orange)/AbPSA (*red*) and *grey* represents PSA-negative classification (adapted with permission from Sun et al. 2007. Copyright 2007 American Chemical Society)

experiment. The unique peaks from each of the two COINs are easily visible in the raw spectrum acquired from the epithelium (Fig. 7.15b, purple spectrum), indicating the presence of both types of COIN at individual spots in the raster. The PSA expression pattern reported for each COIN is shown in Fig. 7.15c, where red and blue indicate classification as PSA positive by (acridine orange)/AbPSA and (basic fuchsin)/AbPSA, respectively, and grey represents classification as PSA negative. Both COINs were detected in almost all spots of the epithelium where tumour is expected. High sensitivity and specificity were achieved in the case of the combination of COINs with two RRMs. Because of COIN's high signal intensity, the tissue binding assay can be conducted using a low concentration ($\sim$30 pM) of COIN-antibody conjugate without the need for secondary amplification and the Raman data can be collected using a relatively low power laser (0.3 mW) and very short signal acquisition times (0.1 s). The single step staining procedure was significantly shorter than traditional immunohistochemistry because steps such as incubation with secondary antibodies, enzymatic colour development time and endogenous biotin blocking are all eliminated (Sun et al. 2007). For multiplex analysis, appropriate mathematical procedures for signal decomposition were employed (Lutz et al. 2008).

Schlücker and co-workers used hydrophilically stabilized Au nanostars with PEG-modified aryl thiols as RRMs for immuno-SERS microscopy on prostate tissue (Schütz et al. 2011). The advantage of Au nanostars is a higher SERS enhancement with the red excitation than for Au spherical NPs. RRMs yielded a complete SAM on the Au nanostar surface. Benign prostate tissue sections were incubated with the antibody-functionalized nanostars. The signature of the SERS label ($\sim$1340 cm^{-1}) was only observed in the basal epithelium, but not in the stroma/connective tissue or lumen (Schütz et al. 2011).

Stone and co-workers reported surface-enhanced spatially offset Raman spectroscopy for detecting NPs deeply in tissue (Stone et al. 2010). Ag NPs labelled with RRMs were injected into the centre of fresh porcine tissue. SERS spectra from these Ag NPs were obtained by spatially offset Raman spectroscopy from a depth of 4.5–5 cm. Later, the same group improved this approach for multiplexed detection and imaging using four different commercial SERS probes (Stone et al. 2011). Each NP suspension was injected into one of the corners of a 10 mm square, from where multiplexed spatially offset Raman spectroscopy imaging of the NPs was obtained according to the characteristic bands of each RRM.

7.7 SERS Medical Applications In Vivo

7.7.1 In Vivo Glucose Sensor

Glucose sensor described above (see Sect. 7.1) was designed even for in vivo transcutaneous glucose sensing on rat models (Stuart et al. 2006). The principle of the sensor is illustrated in Fig. 7.16. Ag FON with mixed SAMs of DT/MH was

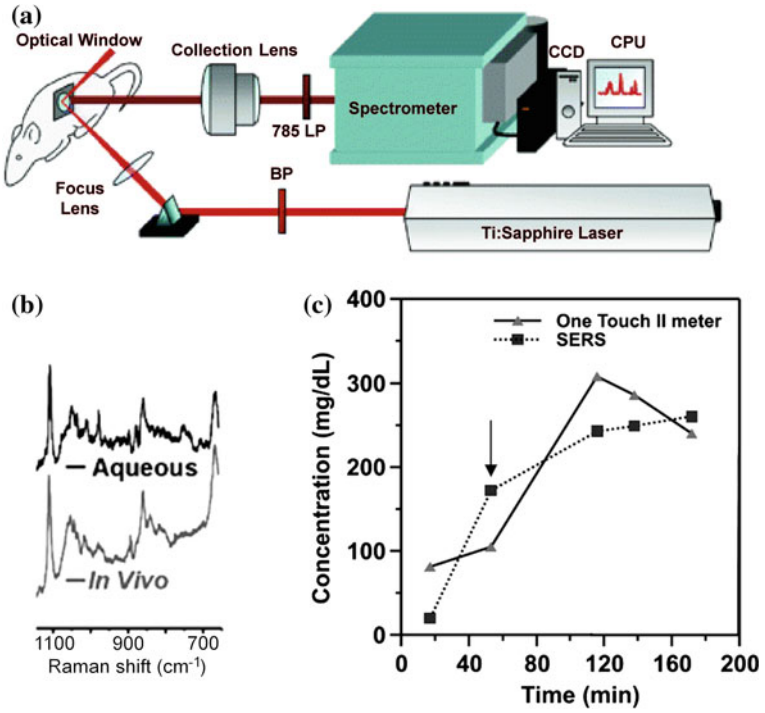

Fig. 7.16 In vivo glucose SERS sensor. **a** Scheme of instrumental apparatus. **b** Typical in vivo spectrum compared to a typical ex vivo spectrum. **c** Time course of the in vivo glucose measurement, *triangles* are measurements made using blood glucometer (One Touch II) and *squares* are measurements made using the SERS sensor. Glucose infusion was started at 60 min, as marked by the *arrow* (adapted with permission from Stuart et al. 2006. Copyright 2006 American Chemical Society)

subcutaneously implanted in a rat so that the glucose concentration of the interstitial fluid could be measured optically through an optical window in the rat's body (Fig. 7.16a). Figure 7.16b shows a typical in vivo spectrum compared to a typical ex vivo spectrum obtained using the same surface and within the same experimental conditions (785 nm excitation, laser power 50 mW, acquisition time 2 min). Figure 7.16c depicts the glucose concentration variation in the rat measured using SERS and the blood glucometer (One Touch II) with respect to time. Both the standard glucometer and the SERS-based measurements effectively tracked the change in glucose concentration. A sharp rise in glucose concentration was detected by both techniques 60 min after the start of the glucose infusion. Moreover, the results demonstrated that glucose binds reversibly to the SERS-active surface and the changes in its concentration as rapidly as 30 s can be tracked. The glucose concentration was monitored in the interstitial fluid of six separate rats. The sensor was able to perform accurately over lower glucose concentrations for 17 days after subcutaneous implantation.

7.7.2 *In Vivo Imaging and Tumour Targeting*

In the last 5–8 years, there has been a progression in the number of studies reporting on in vivo and the clinical use of the SERS spectroscopy (Zavaleta et al. 2011).

The first noninvasive SERS image using a living mouse was reported by Qian and co-workers in 2008 (Qian et al. 2008). Later, Keren and co-workers showed the first SERS image of a whole organ (liver) in a living mouse (Keren et al. 2008). SERS tags, commercial glass-coated Au NPs (Nano-plex Biotags) functionalized with RRM, were injected into the tail vein of a mouse. The mouse was anesthetized on a microscopic table equipped with a horizontal translation stage. This allowed a raster scanning and Raman imaging. SERS images acquired 2 h after injection revealed a bright liver, the primary organ responsible for the natural uptake (because of the reticuloendothelial cells) and excretion of the NPs. This in vivo approach demonstrated ultrasensitive picomolar detection of SERS tags. The maximum depth of penetration for Raman microscope was evaluated by using a tissue mimicking phantom, where a maximum depth of 5.5 mm was observed by using SERS NPs in low (1.3 nM) concentration. Later, Charan and co-workers imaged *Caenorhabditis elegans*—a small, transparent and well characterized nematode—by using bare Ag NPs. SERS signal came preferentially from the lipids and their environment (Charan et al. 2011). This signal was imaged by selecting the spectral range of the CH stretching modes of lipids as an integral signal for imaging. This is one of the very few examples, where intrinsic SERS signatures from the tissue or a cell have been used for whole body Raman imaging. Wang and co-workers monitored the distribution of Au NPs in zebrafish embryos (Wang et al. 2010a). Au NPs were labelled with two different RRMs: 4-MBA and mercaptopyridine. The labelled Au NP tags were microinjected into the one cell stage. SERS spectra were collected from the various regions of the embryos and in different stages of their development.

The first in vivo SERS tumour targeting was reported in previously mentioned work of Qian and co-workers (Qian et al. 2008). Figure 7.17 illustrates this experiment. Single chain variable fragment (scFv) antibodies were conjugated to the Au NPs through heterofunctional thiolated PEG (HS–PEG–COOH) (Fig. 7.17b). It served to recognize the EGFR, which is overexpressed in many types of malignant tumours. Au NPs with core size of 60–80 nm diameter and RRM were components of the SERS tag. The SERS tags were injected into subcutaneous and deep muscular sites in nude mouse (Fig. 7.17a) bearing human head and neck squamous cell carcinoma (Tu686) tumour. A healthy nude mouse received 50 µl of the SERS NP tags (1 nM) by subcutaneous (1–2 mm under the skin) or muscular ($\sim$1 cm under the skin) injection. The subcutaneous spectrum was acquired in 3 s, the muscular spectrum in 21 s and the control spectrum (obtained in an area away from the injection site) also in 21 s. The reference spectrum was acquired from the SERS tags in PBS solution in 0.1 s. The RRM was malachite green with spectral signatures at 427, 525, 727, 798, 913, 1169, 1362, 1581 and 1613 cm^{-1} (Fig. 7.17c). These features were distinct from the Raman signal of animal skin.

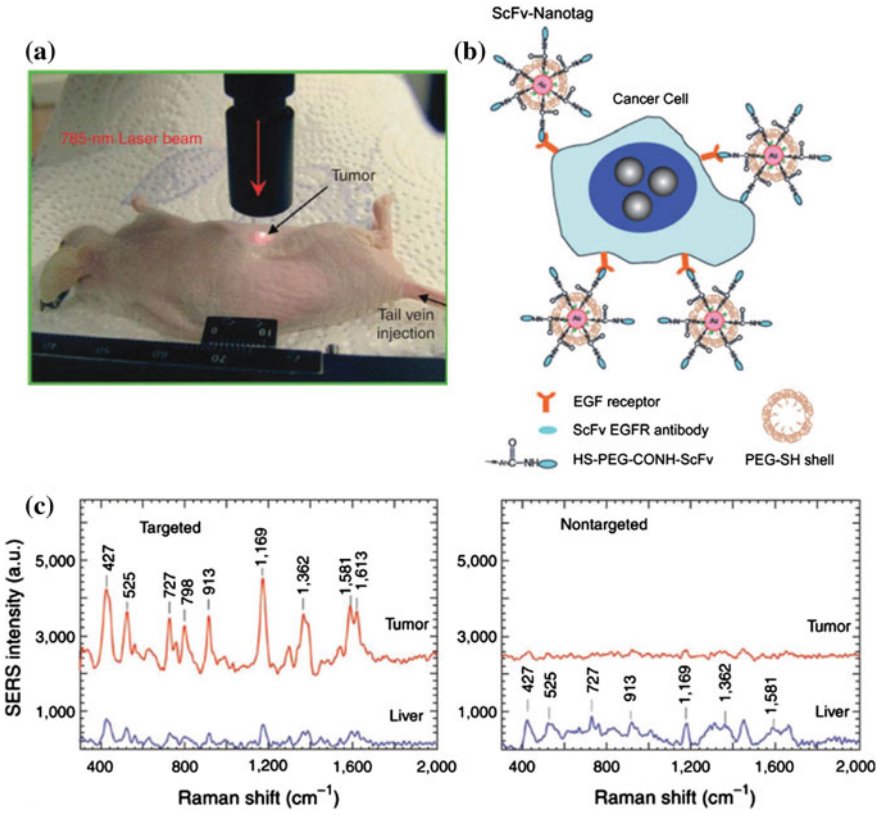

Fig. 7.17 In vivo SERS imaging and cancer targeting. **a** Experimental setup for SERS imaging of tumour of living mouse. **b** Detection scheme and structure of SERS tag for cancer targeting. **c** SERS spectra obtained from the tumour (*red*) and liver (*blue*) by using targeted NPs and nontargeted NPs. The spectra were background subtracted and shifted for better visualization. The RRM is malachite green (adapted with permission from Qian et al. 2008. Copyright 2008 Nature Publishing Group)

In vivo SERS spectra were obtained with a 785 nm excitation (laser power 20 mW). This excitation ensured the minimal optical absorption of water and haemoglobin. SERS signals from approximately 1–2 cm depth in the tissue were acquired. The SERS spectra obtained using targeted NPs demonstrated specific recognition of EGFR-positive tumour sites (Fig. 7.17c) with some nonspecific distribution into liver and spleen, but not into the brain, muscle or other major organs. On the other hand, control experiment using nontargeted NPs proved no SERS signal in tumour region.

The SWNTs were also tested as tumour targeting nanostructures (Keren et al. 2008; Zavaleta et al. 2008). SWNTs have a very small diameter of $\sim$3 nm and a length of 200 nm. Moreover, the high aspect ratio of the carbon structure of SWNTs is ideal for bioconjugation. SWNTs provide intense and inherent Raman peak

(G-band at $\sim$1593 cm^{-1}) which can be tracked in whole body by noninvasive Raman imaging. The results clearly demonstrated that it is possible to examine the distribution and localization of SWNTs in tumour of living mice 24 h after the injection.

The first multiplex imaging of ten different SERS tags upon subcutaneous injection in ten separate areas of a living mouse was reported by Zavaleta et al. (2009). Each SERS tag (Oxonica Materials, Mountain View, CA) consisted of a unique RRM layer adsorbed onto a Au core (60 nm diameter) coated with silica, making the entire diameter of the NP $\sim$120 nm (Fig. 7.18a). 10 separate

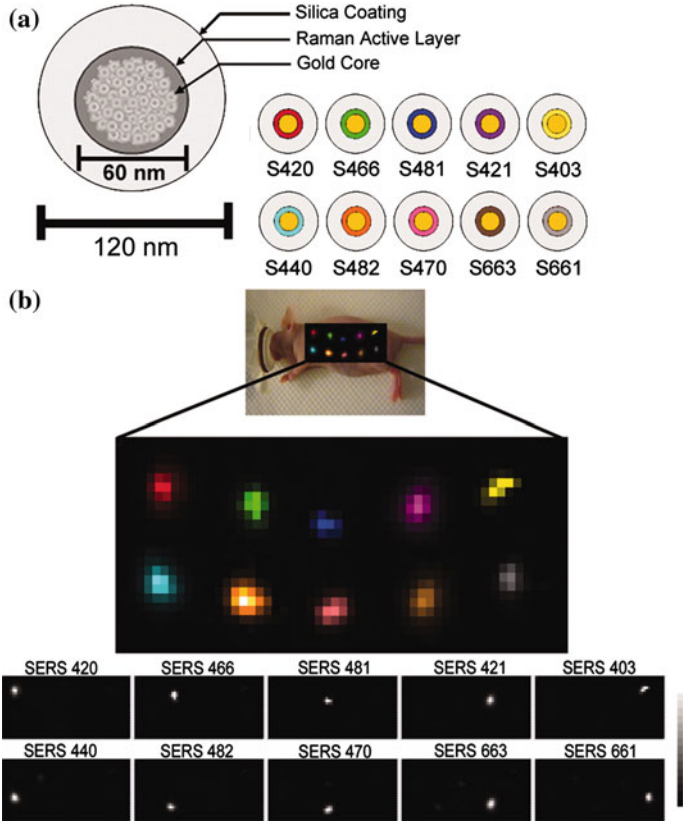

Fig. 7.18 Multiplex in vivo SERS detection using ten different SERS tags. **a** Schematic representation of a SERS tag. To simplify nomenclature, each type of SERS tag is given a three-digit suffix (e.g. S-420) instead of the formal name of the adsorbed RRM. **b** Map of 10 different SERS particles injected in a nude mouse. Arbitrary colours have been assigned to each unique SERS tag batch injected. *Panels below* depict separate channels associated with each of the injected SERS tag. S420, S466, S481, S421, S403, S440, S482, S470, S663 and S661, respectively). Greyscale bar on the *right* depicts the Raman intensity, where *white* represents the maximum intensity and *black* represents no intensity (adapted with permission from Zavaleta et al. 2009. Copyright 2009 The National Academy of Sciences of the USA)

subcutaneous injections of each SERS tag to a nude mouse were carried out and then the entire area of interest was mapped with a Raman microscope. The map was then analysed with postprocessing software, where preassigned reference spectra of each SERS tag were used to determine the best spectral fit with their corresponding SERS tag. The software then separated out intensity maps into various channels showing where in the map each SERS tag was detected. The resulting image showed all 10 injections correctly separated out into their corresponding spectral channel with minimal overlap among the channels (Fig. 7.18b). These results demonstrated a great potential for multiplexed imaging in living subjects. It can be particularly useful when multiple biomarkers associated with a specific disease should be detected.

Dinish and co-workers reported the targeted multiplex detection of intrinsic cancer biomarkers in MDA-MB-231 breast cancer cell line and in a murine xenograft model (Dinish et al. 2014). Three biocompatible SERS tags were constructed with Au NPs and three RRMs: Cy5, malachite green isothiocyanate and RH6G. The SERS tags were further conjugated with antibodies against EGFR, CD44 and TGF beta receptor II cancer biomarkers. EGFR is the cell's surface receptor for members of the EGFR family of extracellular protein ligands. It is a prognostic marker in many types of cancers including breast cancer. CD44 is a major cell surface adhesion molecule and is a receptor for the glycosaminoglycan, hyaluronan. It plays an important role in tumour growth and metastasis. Down regulation of TGF beta receptor II is a key step in breast carcinogenesis. In the case of in vitro experiment with cancer cells, SERS spectra from the cells showed the fingerprint Raman peak from each SERS tag bound to corresponding biomarker on the cell surface: 1120 cm^{-1} of Cy5, 1175 cm^{-1} of malachite green isothiocyanate and 1650 cm^{-1} of RH6G. SERS intensity map image demonstrated the expression and relative distribution of the cancer biomarkers on the cell surface bound to the antibody conjugated SERS tags, Cy5, malachite green isothiocyanate and RH6G respectively. In vivo multiplex detection was carried out by injecting 200 μl of the three bioconjugated SERS tags into the centre of the tumour on a subcutaneous MDA-MB-231 breast cancer xenograft mouse model. Xenograft is a surgical graft of tissue from one species to an unlike species. The results showed that intratumourally injected SERS tags specifically targeted the three biomarkers. SERS spectra of RRMs exhibited maximum signal at 6 h and no detectable signal at 72 h. However, SERS tags without antibodies showed no detectable signal after 6 h. This difference could be due to the specific binding of the bioconjugated SERS tags to the receptors on the cell surface.

The major problem of in vivo SERS detection/imaging comes from the limited penetration depth (in the range of few mm) of biological objects. This can be partly solved using NIR-IR excitation (typically 785 nm) where optical penetration in tissue is maximized. Therefore, employing NIR-IR resonance excitation of both metallic nanostructure and RRM in SERS tag can substantially enhance the SERS signal and thus increase sensitivity. The most common RRMs such as CV and R6G are more efficient in the visible region. Small Ag NPs and Au NPs have also limited LSPR in NIR-IR region. Thus, the new SERS tags with spectral properties in the

NIR-IR range are definitely required for in vivo SERS applications. The Au NRs or Au nanostars (Rodríguez-Lorenzo et al. 2011) were found to be suitable nanostructures providing high SERS enhancement in NIR-IR. Au NRs coated with PEG polymers and various RRMs were presented as an efficient platform for multiplex in vivo SERS detection within NIR-IR excitation (Qian et al. 2011; von Maltzahn et al. 2009; Jokerst et al. 2012). Au NRs were found to be highly stable, to be detectable down to femtomolar concentrations and to have low baseline cytotoxicity (von Maltzahn et al. 2009).

Concerning RRMs, Samanta and co-workers synthesized a series of tricarbocyanine derivatives with NIR absorption properties and ultrasensitive SERS in vivo cancer detection (Samanta et al. 2011). Their SERS efficiency was compared with those of Au NPs (60 nm diameter). Among them, CyNAMLA-381, which displayed about 12× higher sensitivity than the standard DTTC, was chosen as the best RRM (Fig. 7.19). SERS tags with this RRM and BSA and glutaraldehyde protective layer were used for in vivo cancer detection. The SERS tag was functionalized with HER2-recognition antibodies (anti-HER2 monoclonal antibody or scFv anti-HER2 antibody). Such SERS tags were injected into nude mice bearing xenografts generated from SK-BR-3 cells. After 5 h, SERS spectra from the tumour site perfectly resembled the SERS spectra of the tag (Samanta et al. 2011). The same group later developed the SERS tags with two new NIR RRMs—Cy7LA and Cy7.5LA—as a partner with recently synthesized CyNAMLA-381 for multiplexing (Maiti et al. 2012). These SERS tags possess excellent SERS signal stability over a period of 1 month. As a proof of concept for multiplex targeted in vivo detection, they successfully demonstrated the simultaneous sensing of cancer in a living mouse using these three bioconjugated SERS tags.

Recently, a new class of ultra sensitive, NIR RRMs—2-thienyl-substituted chalcogenopyrylium dye—was synthesized (Harmsen et al. 2015b). The 2-thienyl

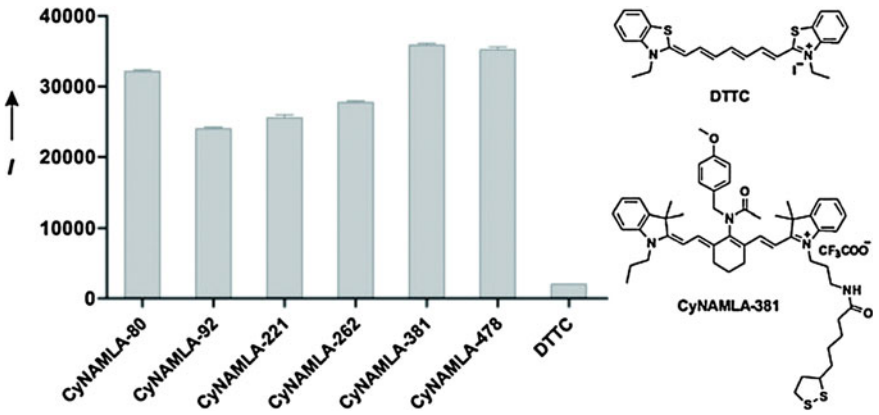

Fig. 7.19 SERS intensity of selected BSA-encapsulated-tricarbocyanine derivatives on 60 nm Au NPs recorded using 785 nm excitation (reproduced with permission from Samanta et al. 2011. Copyright 2011 Wiley-VCH Verlag GmbH & Co. KGaA, Weinheim)

group is not only part of the dye chromophore, but also can be rigorously coplanar with the rest of the chromophore. This allows the dye molecules to be in close proximity to the NP surface creating higher SERS. Thus, when adsorbed onto Au NPs, these dyes produce biocompatible SERS tags with unprecedented LOD about 100 aM. Ex vivo multiplexed Raman imaging of the tumour showed that the SERRS signals from two different EGFR-targeted SERS tags were more intense for the tumour site than for the surrounding tissue. It was a proof of selective localization of SERS tags at the tumour site. The low LOD in combination with the high resolution of Raman imaging enabled highly sensitive and specific real-time tumour targeting, as a result of the fingerprint spectra of the different SERS tags. This can offer multiplexed disease marker detection in vivo (Harmsen et al. 2015b). Similarly, SERS tags operating with 1280 nm excitation were constructed from RRMs selected from a library of 14 chalcogenopyrylium dyes containing phenyl, 2-thienyl and 2-selenophenyl substituents and of hollow Au HNSs (Bedics et al. 2015). These SERS tags are unique as they have multiple chalcogen atoms available which allow them to adsorb strongly onto the surface of the Au HNSs thus producing exceptional SERS signals at this long excitation wavelength. LODs about pM were obtained and individual RRMs of the library were identified by PCA and classified according to their unique structure and SERS signature.

Another issue of SERS tags for in vivo biomedical applications is that it requires efficient uptake of SERS tags, long circulation times and high stability. To date, silication of a dye-adsorbed NP has been most effective in retaining in vivo SERS tag stability and biocompatibility (Wang et al. 2013c). Current silication methods depend on high dye-metal affinities, which can be limited by unfavourable electrostatic interactions. Sulphur-containing dyes with affinities to gold are available, but scaling up the silication process can also often lead to size variation, aggregation and uncontrollable dye incorporation. The silica layer also approximately doubles the size of the metallic core that limits the synthesis of SERS NPs of the smaller size necessary for a variety of biomedical applications. This can be overcome if hydrophilic polymers surface coatings are employed. The synthesis of these SERS tags includes treating dye-adhered metallic NPs with thiolated-PEG or analogous polymers. However, competition for vacant binding sites can limit signal intensities and/or polymer grafting densities (Wang et al. 2013c). Iacono and co-workers reported a new hydrophilic NIR dye-loaded poly(N-(2-hydroxypropyl) methacrylamides) polymer and their application for Au NPs-based SERS imaging of lymph nodes (Iacono et al. 2014). The integration of various SERS RRMs into a biocompatible polymeric surface coating allowed for controlled dye incorporation, high colloidal stability and optimized in vivo circulation times. This technique led to the synthesis of very small (<20 nm) SERS tags but depending on their size, the NPs can emit both SERS and fluorescence. Au NPs covered by poly(N-(2-hydroxypropyl)methacrylamides) polymer showed longer in vivo signal stability in a 24 h period compared to coated particles assembled with noncovalent gold-dithioester chelate interactions.

Dong and co-workers reported the use of acupuncture needles as a carrier of SERS-active NPs (Dong et al. 2011). The SERS-active needles were fabricated

from commercial stainless-steel acupuncture needles of 0.2 mm in diameter. They were first incubated with 3-mercaptopropyltriethoxysilane and then the SERS-active NPs, comprising a thin Au shell coated on a dielectric core, were assembled on the needle surface. When the needle was inserted into the body, interstitial fluids would diffuse into the gaps between the attached NPs. Then, the needle was pulled out and analytes in the fluids were taken out for SERS measurement. The ability of in vivo SERS detection was assessed by using 6-mercaptopurine (6-MP). Its aqueous solution was injected into the ear vein of anesthetized New Zealand rabbit. Then, two SERS-active needles were inserted into the other ear vein and *vastus lateralis* tendon (removed with scissors) to detect the drug concentration in the blood and muscles, respectively. SERS measurement was carried out immediately after the needle was pulled out. The results indicated that the concentration of free 6-MP in the body decreased after injection and the concentration of 6-MP in the blood is higher than that in muscles.

7.7.3 Clinical Utility of SERS

7.7.3.1 Surgery Guidance of Brain Tumours

Delineation of tumour margins is very important for better treatment of patients with tumours. Surgery remains a mainstay in the treatment of brain tumours, in particular glioblastoma multiforme. Incomplete tumour resections lead to tumour recurrence at 80−90 % patients (Oh et al. 2011). Different imaging techniques are currently being utilized to better visualize tumour margins. 3D imaging with high spatial resolution (photoacoustic) in combination with SERS imaging of Au NRs was used for detection and resection guidance of ovarian cancer in living mice (Jokerst et al. 2012). The same group proposed multimodal probe based on a single imaging agent, whole brain tumour localization by MRI, 3D imaging with high spatial resolution (photoacoustic) and high-resolution surface imaging of tumour margins by SERS (Kircher et al. 2012). Here, the SERS tags containing a 60 nm Au core modified with the RRM (*trans*-1,2-bis(4-pyridyl)-ethylene) and a protective silica shell were injected in glioblastoma-bearing mice. The SERS signal helped in identifying microscopic tumour and its resection in vivo. Since the NPs did not carry any tumour targeting molecule, the authors speculated that the NPs would enter the extravascular space by diffusion through the disrupted blood-brain barrier and accumulate in cells within the brain tumour because of enhanced permeability and retention effect.

Harmsen and co-workers presented the precise visualization of the full tumour extent in transgenic mouse models of breast cancer, sarcoma, pancreatic ductal adenocarcinoma and prostate cancer (Harmsen et al. 2015a). Their SERRS tag has the following features: (i) star-shaped Au core (75 nm diameter) demonstrating a LSPR in the NIR region, (ii) a RRM that is in resonance with the detection laser (785 nm) and (iii) a biocompatible encapsulation method that allows efficient

loading of the resonant RRM at the Au surface. The Au nanostars were coated with silica in the presence of the resonant RRM IR-780 perchlorate without the need for any surface primers. SERRS nanostars generated photostable SERRS signal with a LOD of 1.5 fM in solution under conditions that are close to those required for clinical translation (100 mW laser power, 1.5 s acquisition time, 5× objective). They showed also a high degree of batch-to-batch consistency with minimal variation in SERRS signal intensity (±4.5 % coefficient of variation) (Harmsen et al. 2015a). Bifunctional NPs comprising a superparamagnetic material and a plasmonic metal were also used in both MRI and SERS (Yigit et al. 2011). The bifunctional Au/iron NPs embedded with the RRM DTTC and PEG protective shell were injected into the muscle of a living mouse for in vivo MRI and SERS detection. SERS detection was performed directly in the injection area. Both spectra from the living mouse and excised muscle tissue (excised after in vivo detection) showed the same spectral feature as the DTTC SERS spectrum obtained in solution (Harmsen et al. 2015a).

However, MRI is costly and a time-consuming method. Moreover, it was found that the assessment of tumour borders by MRI was often incongruent with the actual tumour borders due to the brain shift during surgery. To overcome this limitation, Karabeber and co-workers developed an intraoperative tumour detection method that could be applied clinically in the near future (Karabeber et al. 2014). It combines static SERS imaging and real-time SERS NP detection using a hand-held Raman scanner during surgery. This was accomplished in a genetic mouse model that closely mimics the pathology of human glioblastoma multiforme. The SERS tags formed by Au core, RRM (4,4′-dipyridyl) and silica shell were allowed to circulate for 24 h in the mouse to ensure that they accumulated in the tumours. Tumour tissue was detected in situ with the hand-held Raman scanner using 785 nm laser line as excitation. Figure 7.20 shows the residual brain tumour before resection (a) and subsequently resected (b) and corresponding SERS spectra (c). SERS signal of RRM was observed only in the case of a tumour present while no SERS signal appeared in normal tissue. The presence of SERS tags within the resected specimen was proved by TEM. Immunohistochemical staining for the tumour marker Olig-2 confirmed that the resected tissue indeed represented microscopic glioblastoma multiform cancer spread. Importantly, the hand-held scanner was able to identify in 10 mice small tumour spots that were not detected on the Raman images. This is attributable to the flexibility of angulating hand-held scanner to probe any area in the operating bed, even those located at the lateral margins underneath overlying normal brain tissue. Therefore, SERS-guided surgery using a hand-held Raman scanner represents a highly translatable approach to facilitate the resection of brain tumours and potentially other cancer types. It also provides the capability of scanning the operative bed from any desired angle in order to examine every aspect of the tumour bed. One of the limitations of this approach is that it was performed on brains that had been fixed in paraformaldehyde and is therefore not fully representative of the actual surgical environment. Another potential limitation

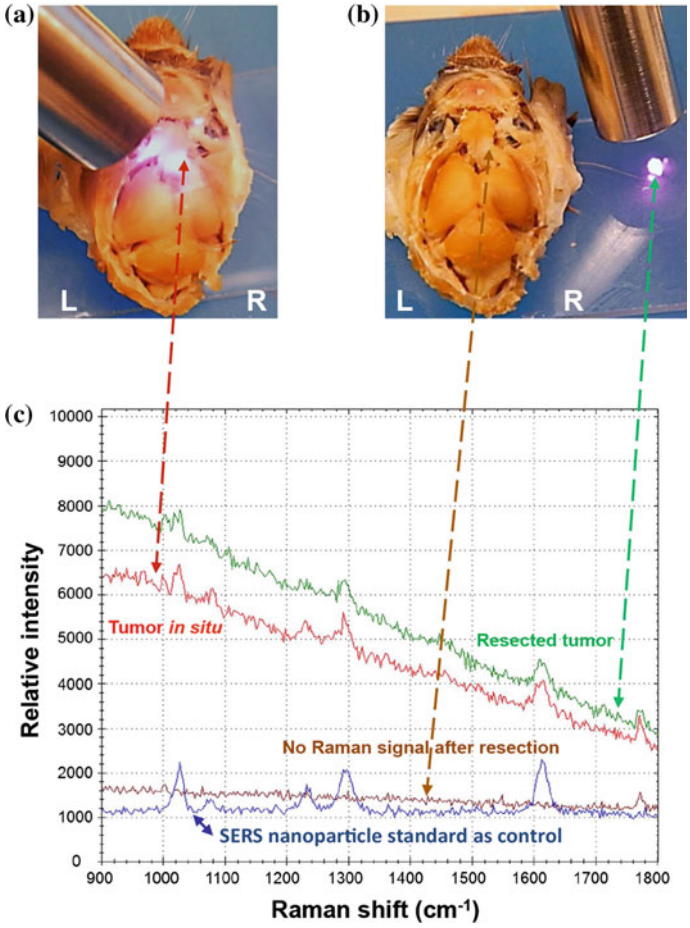

Fig. 7.20 In situ SERS-NP-guided surgery of brain tumour using hand-held Raman scanner. The tumour tissue before resection (**a**), after resection (**b**) and corresponding SERS signal coming from SERS tags (**c**) (adapted with permission from Karabeber et al. 2014. Copyright 2014 American Chemical Society)

of the technique is that depth penetration with conventional Raman spectroscopy imaging techniques is in the order of few mm.

7.7.3.2 Endoscopic Imaging Using SERS

Endoscopic imaging is an invaluable diagnostic tool allowing minimally invasive access to tissues deep within the body. It has played a key role in screening colon cancer and is credited with preventing deaths through the detection and removal of precancerous polyps. Because of limited depth of penetration associated with most

optical techniques, endoscopic approach in attempting to translate Raman spectroscopy to clinical use was tested. In 2000, Shim and co-workers reported the first in vivo Raman spectroscopy of human gastrointestinal tissues measured during a routine clinical endoscopy (Shim et al. 2000). This was achieved by using a NIR fibre-optic Raman probe that was passed through the endoscope instrument channel and placed in contact with the tissue surface. Thus far, it was possible to evaluate intrinsic tissue signals using contact endoscopic Raman probes. However, another strategy currently being developed could exploit ultrasensitive detection of using endoscopic SERS molecular imaging agents to diagnose cancer in vivo (Zavaleta et al. 2011). SERS-endoscopic strategy for colon cancer detection involves three basic steps: (i) topical administration of tumour-targeted SERS-active NPs to a particular area of interest during endoscopy followed by washing of the unbound NPs, (ii) utilization of Raman endoscopic device as it is deployed through the working channel of a commercial endoscope to detect and quantify the presence of the bound targeted NPs relative to internal controls and (iii) interpretation of results in real-time to determine what pathological conditions exist based on SERS signal associated with tumour-targeted NPs (Zavaleta et al. 2011). Several groups have developed a fibre-based, noncontact Raman endoscope to interrogate SERS NPs as contrast agents (Mohs et al. 2010; McVeigh et al. 2012; Zavaleta et al. 2013; Wang et al. 2014).

Zavaleta and co-workers reported first SERS-based multiplexing using commercial SERS tags (Cabot Security Systems) consisting of 10 different RRMs adsorbed onto a Au core (60 nm diameter) and then coated with silica (Zavaleta et al. 2013; Garai et al. 2013). The Raman endoscopic device was equipped with a flexible fibre bundle with a centrally located single-mode fibre for illumination at 785 nm and an additional 36 surrounding multimode fibres for light collection. Characterization of the Raman instrument was performed with SERS tags on excised human tissue samples and it has shown unsurpassed sensitivity and multiplexing capabilities, detecting 326 fM concentration of NPs and unmixing 10 variations of colocalized SERS tags. Another unique feature of this noncontact Raman endoscope is that it has been designed for efficient use over a wide range of working distances from 1 to 10 mm.

As a point-detection device, images could only be created on-the-bench by physically moving the sample, which is not a viable approach for in vivo imaging of large, complex surfaces. Recently, Garai and co-workers reported the design and in vivo application of a miniature, noncontact, opto-electro-mechanical Raman endoscopic device (Garai et al. 2015). The concept is illustrated in Fig. 7.21. The device was designed such that it can be inserted through the accessory channel of a clinical endoscope. As the endoscope was being retracted in the gastrointestinal tract, the device simultaneously scanned the lumen and the collected SERS signal from SERS tags was analysed (Fig. 7.21a). Figure 7.21b shows a scheme of the distal end of the device. A brushless DC motor that rotates a mirror caused the collimated beam to sweep 360°, enabling luminal imaging of the colon wall. The device was not required to be in contact with the tissue, which was enabled through the use of the collimated illumination beam. A custom, miniature, concentrically

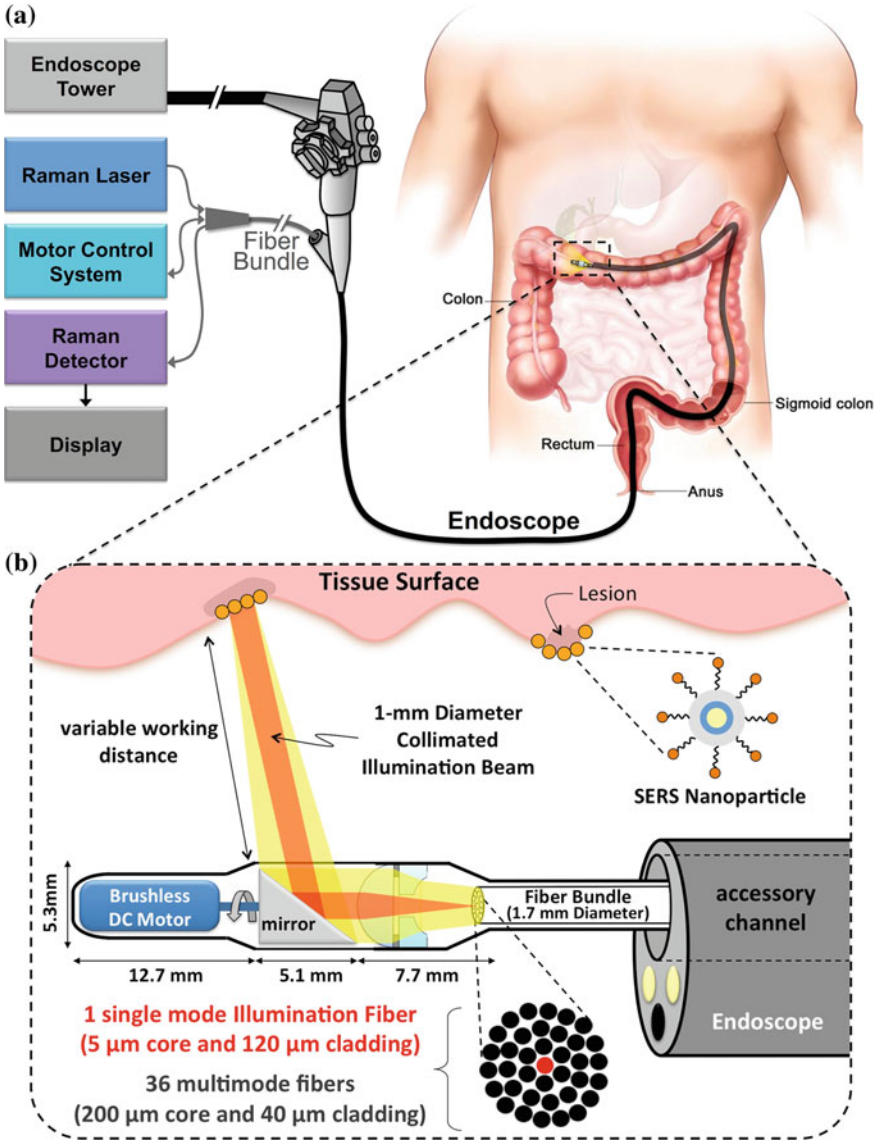

Fig. 7.21 Endoscopic SERS molecular imaging. **a** The scheme of the basic concept. **b** Expanded scheme of the distal end of the device. See text for details (adapted from Garai et al. 2015. Copyright 2015 Garai et al.)

segmented, air-spaced doublet lens having a nonreciprocal optical path consists of a plano-convex lens and an adjacent plano-concave lens with a central hole. The doublet lens increased collection efficiency at longer, clinically relevant working distances. This device enabled rapid scanning of topologically complex luminal

surfaces of hollow organs (e.g. colon and esophagus) and produced quantitative images of the relative concentrations of present SERS tags. This approach can also provide multiplexed information via a panel of SERS tags. Human studies demonstrated the speed and simplicity of this technique. A male patient undergoing routine colonoscopy screening consented to participate in the study. A signal was acquired over 30 s and no intrinsic Raman signal from the tissue was detected. Therefore, this new screening strategy has the potential to improve diagnosis and to guide therapy by enabling sensitive quantitative molecular detection of small and otherwise hardly detected lesions in the context of white light endoscopy.

7.7.4 *Intracellular SERS Monitoring of Drug Release In Vivo*

Thiopurine analogues represent potential antileukaemic and antineoplastic drugs for the treatment of many cancer diseases. Ock and co-workers employed label-free SERS and live cell imaging techniques to in vitro and in vivo study of uptake and release of thiopurine drugs (Ock et al. 2012). The main principle of this study is illustrated in Fig. 7.22. 6-MP and 6-thioguanine (6-TG) adsorbed on the surface of Au NPs were replaced by glutathione monoester (GSH–OEt) as an intracellular external stimulus (Fig. 7.22a). The release of a portion of 6-MP or 6-TG molecules from the Au NPs was proved by a decrease of their SERS signal. A tripeptide with a methyl group instead of a thiol group was used as an inactive GSH derivative in a negative control experiment. In vivo SERS studies were carried out by subcutaneous injection of 6-TG modified Au NPs in living nude mice. The SERS intensity of 6-TG decreased upon GSH–OEt injection, whereas the control tripeptide did not show a significant influence (Fig. 7.22b). A live cell imaging technique provided a nanomolar range release of thiopurine from Au NP surfaces after the injection of external glutathione.

Conde and co-workers developed Au NP conjugates labelled with a RRM and the commercial antibody-drug conjugate Cetuximab (Erbitux®) for targeted detection and treatment of tumours in vivo (Conde et al. 2014). Mice models were implanted with cancerous cells to generate xenografts and the mice were then treated with nanostructures via tail injection, while the tumours were located in the right leg. The conjugates were successfully translocated to the tumour site and resulted in a reduction of further tumour development by the inhibition of cellular division. Active targeting of the tumour was monitored via SERS and large SERS signals were observed in mice treated with the drug conjugates whilst minimal signals were observed from those treated with drug-free nanostructures. The authors reported that the signals measured from drug labelled NPs at the xenograft were 4.5× higher than those of the drug-free system as measured from a key identification peak at 508 cm^{-1}.

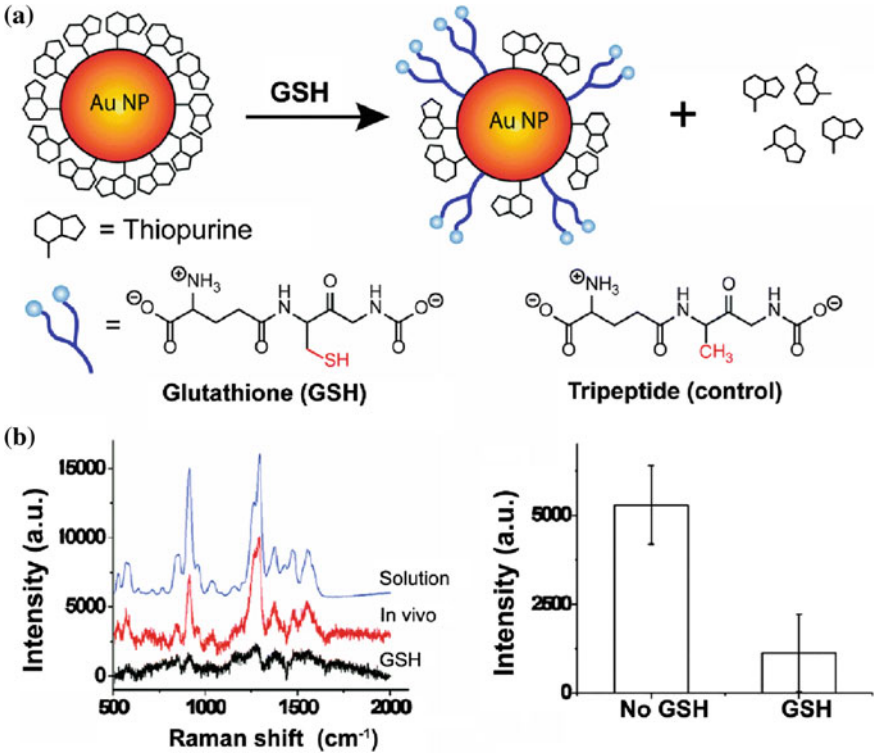

Fig. 7.22 SERS study of uptake and release of thiopurine drugs. **a** GSH-mediated release of thiopurines adsorbed on Au NPs. **b** In vivo SERS spectra of 6-TG adsorbed on Au NPs after treatment of GSH and the corresponding stick diagram of results obtained with and without GSH treatment (adapted with permission from Ock et al. 2012. Copyright 2012 American Chemical Society)

The expression of adhesion molecules such as intercellular adhesion molecule 1 (ICAM-1) by endothelial cells is crucial during acute inflammation. In vivo SERS detection of (ICAM-1) expression on endothelial cells was reported by using SERS tags injected into live mice (McQueenie et al. 2012). SERS tags consist of Au NPs with RRMs encapsulated with a silica shell and then conjugated to anti-ICAM-1 antibody to target ICAM-1 expressed in mice. ICAM-1 expression was induced by local lipopolysaccharide injection in the ear of mice. Approximately 24 h after the intradermal local lipopolysaccharide injections, an intravenous injection of the SERS labels was performed. SERS spectra were measured 30 min after the injection of the SERS tags. SERS spectra recorded from the ears of mice injected with anti-ICAM-1 NPs reproduced spectral features corresponding to the neat SERS tag. The authors also demonstrated that SERS tags provide higher detection sensitivity for ICAM-1 in comparison with a conventional fluorescence probe and offer improvements in terms of depth resolution and signal-to-noise ratio.

7.7.5 *Toxicity Issue*

The long-term toxicity of metallic NPs inside the human body is not fully explored. Toxicity studies of developing systems, organisms or individual differentiating cells provide particular challenges for in vivo SERS applications. The biocompatibility of Ag NPs is not as good as that of Au NPs because of silver's oxidative nature, which drives genotoxic and cytotoxic outcomes (AshaRani et al. 2009). The biocompatibility of metallic NPs is dependent on several factors, including metal type, shape, size and capping materials. In general, ultrasmall Au nanoclusters have greater cytotoxic effects due to their strong endocytosis effectiveness and binding ability to B-form DNA (Jiang et al. 2008). However, the Au NPs about 30–100 nm diameter that are commonly used as SERS substrates cause no noticeable toxicity at concentrations up to 100 mM (Jiang et al. 2008).

Generally, it is necessary to use the lowest possible concentration of Au NPs. This can be achieved only at optimal sensitivity conditions such as using RRMs and SERS tags providing maximal SERS signal in NIR IR. The biocompatibility of PEGylated Raman-active Au NPs was investigated using human cells. No cytotoxicity occurred in either HeLa (human cervical cancer cells) or HepG2 (human liver cancer cells) cell lines in the acute setting (Thakor et al. 2011a). Physical redistribution of NPs in time can change their cytotoxicity with developmental stage. After prolonged exposures (48 h) at relatively high concentrations (1000 NPs per cell), a minimal amount of cytotoxicity was seen in both cell lines because of increases in cellular oxidative stress (Thakor et al. 2011a). Surface coating is also a key factor that determines the biocompatibility of NPs. The biocompatibility of cytotoxic NPs can be greatly increased by using proper coating materials. For example, reduced cytotoxicity was reported after the removal (Wang et al. 2010b) or replacement (Boca and Astilean 2010) of toxic surfactants from metallic nanostructures (e.g. Au NRs) with amino groups or polymers that stabilize the particles while minimizing their toxic effects. Silica-coating which is often used to stabilize the SERS tag also reduces the toxicity of Au NPs and favours them for in vivo applications (Thakor et al. 2011b).

References

J.L. Abell, J.M. Garren, J.D. Driskell, R.A. Tripp, Y. Zhao, Label-free detection of micro-RNA hybridization using surface-enhanced Raman spectroscopy and least-squares analysis. J. Am. Chem. Soc. **134**, 12889 (2012)

L.R. Allain, T. Vo-Dinh, Surface-enhanced Raman scattering detection of the breast cancer susceptibility gene BRCA1 using a silver-coated microarray platform. Anal. Chim. Acta **469**, 149 (2002)

P.V. AshaRani, G. Low Kah Mun, M.P. Hande, S. Valiyaveettil, Cytotoxicity and genotoxicity of silver nanoparticles in human cells. ACS Nano **3**, 279 (2009)

Š. Bálint, S. Rao, M. Marro, P. Miškovský, D. Petrov, Monitoring of local pH in photodynamic therapy-treated live cancer cells using surface-enhanced Raman scattering probes. J. Raman Spectrosc. **42**, 1215 (2011)

M.A. Bedics, H. Kearns, J.M. Cox, S. Mabbott, F. Ali, N.C. Shand, K. Faulds, J.B. Benedict, D. Graham, M.R. Detty, Extreme red shifted SERS nanotags. Chem. Sci. **6**, 2302 (2015)

L. Beqa, Z. Fan, A.K. Singh, D. Senapati, P.C. Ray, Gold nano-popcorn attached SWCNT hybrid nanomaterial for targeted diagnosis and photothermal therapy of human breast cancer cells. ACS Appl. Mater. Interfaces **3**, 3316 (2011)

S.C. Boca, S. Astilean, Detoxification of gold nanorods by conjugation with thiolated poly (ethylene glycol) and their assessment as SERS-active carriers of Raman tags. Nanotechnology **21**, 235601 (2010)

Y.C. Cao, R. Jin, C.A. Mirkin, Nanoparticles with Raman spectroscopic fingerprints for DNA and RNA detection. Science **297**, 1536 (2002)

S. Charan, F.C. Chien, N. Singh, C.W. Kuo, P. Chen, Development of lipid targeting Raman probes for in vivo imaging of caenorhabditis elegant. Chem.–Eur. J **17**, 5165 (2011)

R. Chen, J. Lin, S. Feng, Z. Huang, G. Chen, J. Wang, Y. Li, H. Zeng, Applications of SERS spectroscopy for blood analysis, in *Applications of Raman Spectroscopy to Biology—From Basic Studies To Disease Diagnosis*, ed. by M. Ghomi (IOS Press, Amsterdam, 2012a), pp. 72–105

Y. Chen, G. Chen, S. Feng, J. Pan, X. Zheng, Y. Su, Y. Chen, Z. Huang, X. Lin, F. Lan, R. Chen, H. Zeng, Label-free serum ribonucleic acid analysis for colorectal cancer detection by surface-enhanced Raman spectroscopy and multivariate analysis. J. Biomed. Opt. **17**, 067003 (2012b)

X. Chen, Z. Huang, S. Feng, J. Chen, L. Wang, P. Lu, H. Zeng, R. Chen, Analysis and differentiation of seminal plasma via polarized SERS spectroscopy. Int. J. Nanomed. **7**, 6115 (2012c)

Y. Chen, X. Zheng, G. Chen, C. He, W. Zhu, S. Feng, G. Xi, R. Chen, F. Lan, H. Zeng, Immunoassay for LMP1 in nasopharyngeal tissue based on surface-enhanced Raman scattering. Int. J. Nanomed. **7**, 73 (2012d)

I. Choi, Y. Huh, D. Erickson, Ultra-sensitive, label-free probing of the conformational characteristics of amyloid beta aggregates with a SERS active nanofluidic device. Microfluid. Nanofluid. **12**, 663 (2012)

H. Chon, S. Lee, S.Y. Yoon, S.I. Chang, D.W. Lim, J. Choo, Simultaneous immunoassay for the detection of two lung cancer markers using functionalized SERS nanoprobes. Chem. Commun. **47**, 12515 (2011)

H. Chon, S. Lee, S.Y. Yoon, E.K. Lee, S.I. Chang, J. Choo, SERS-based competitive immunoassay of troponin I and CK-MB markers for early diagnosis of acute myocardial infarction. Chem. Commun. **50**, 1058 (2014)

I.H. Chou, M. Benford, H.T. Beier, G.L. Cote, M. Wang, N. Jing, J. Kameoka, T.A. Good, Nanofluidic biosensing for beta-amyloid detection using surface enhanced Raman spectroscopy. Nano Lett. **8**, 1729 (2008)

I. Chourpa, F.H. Lei, P. Dubois, M. Manfait, G.D. Sockalingum, Intracellular applications of analytical SERS spectroscopy and multispectral imaging. Chem. Soc. Rev. **37**, 993 (2008)

J. Conde, C. Bao, D. Cui, P.V. Baptista, F. Tian, Antibody-drug gold nanoantennas with Raman spectroscopic fingerprints for in vivo tumour theranostics. J. Control. Release **183**, 87 (2014)

U.S. Dinish, G. Balasundaram, Y.T. Chang, M. Olivo, Actively targeted in vivo multiplex detection of intrinsic cancer biomarkers using biocompatible SERS nanotags. Sci. Rep. **4**, 4075 (2014)

F.T. Docherty, P.B. Monaghan, R. Keir, D. Graham, W.E. Smith, J.M. Cooper, The first SERRS multiplexing from labelled oligonucleotides in a microfluidics lab-on-a-chip. Chem. Commun. **1**, 118 (2004)

J. Dong, Q.F. Chen, C.H. Rong, D.Y. Li, Y.Y. Rao, Minimally invasive surface-enhanced Raman scattering detection with depth profiles based on a surface-enhanced Raman scattering-active acupuncture needle. Anal. Chem. **83**, 6191 (2011)

J.A. Dougan, D. MacRae, D. Graham, K. Faulds, DNA detection using enzymatic signal production and SERS. Chem. Commun. **47**, 4649 (2011)

J.D. Driskell, R.A. Tripp, Label-free SERS detection of microRNA based on affinity for an unmodified silver nanorod array substrate. Chem. Commun. **46**, 3298 (2010)
A.M. Fales, H.T. Yuan, Vo-Dinh, Silica-coated gold nanostars for combined surface-enhanced Raman scattering (SERS) detection and singlet-oxygen generation: a potential nanoplatform for theranostics. Langmuir **27**, 12186 (2011)
A.M. Fales, H.T. Yuan, Vo-Dinh, Cell-penetrating peptide enhanced intracellular Raman imaging and photodynamic therapy. Mol. Pharmaceutics **10**, 2291 (2013)
A. Farhadi, A. Roxin, B.C. Wilson, G. Zheng, Nano-enabled SERS reporting photosensitizers. Theranostics **5**, 469 (2015)
K. Faulds, F. McKenzie, W.E. Smith, D. Graham, Quantitative simultaneous multianalyte detection of DNA by dual-wavelength surface-enhanced resonance Raman scattering. Angew. Chem. Int. Ed. **46**, 1829 (2007)
K. Faulds, R. Jarvis, W.E. Smith, D. Graham, R. Goodacre, Multiplexed detection of six labelled oligonucleotides using surface enhanced resonance Raman scattering (SERRS). Analyst **133**, 1505 (2008)
S. Feng, R. Chen, J. Lin, J. Pan, G. Chen, Y. Li, M. Cheng, Z. Huang, J. Chen, H. Zheng, Nasopharyngeal cancer detection based on blood plasma surface-enhanced Raman spectroscopy and multivariate analysis. Biosens. Bioelectron. **25**, 2414 (2010)
S.Y. Feng, R. Chen, J.Q. Lin, J. Pan, Y. Wu, Y.Z. Li, J. Chen, H. Zeng, Gastric cancer detection based on blood plasma surface-enhanced Raman spectroscopy excited by polarized laser light, Biosens. Bioelectron. **26**, 3167 (2011)
S. Feng, D. Lin, J. Lin, B. Li, Z. Huang, G. Chen, W. Zhang, L. Wang, J. Pan, R. Chen, H. Zeng, Blood plasma surface-enhanced Raman spectroscopy for non-invasive optical detection of cervical cancer. Analyst **138**, 3967 (2013)
S. Feng, S. Huang, D. Lin, G. Chen, Y. Xu, Y. Li, Z. Huang, J. Pan, R. Chen, H. Zeng, Surface-enhanced Raman spectroscopy of saliva proteins for the noninvasive differentiation of benign and malignant breast tumors. Int. J. Nanomed. **10**, 537 (2015)
R.A. Ferguson, H. Yu, M. Kalyvas, S. Zammit, E.P. Diamandis, Ultrasensitive detection of prostate-specific antigen by a time-resolved immunofluorometric assay and the immulite(R) immunochemiluminescent third-generation assay: Potential applications in prostate and breast cancers. Clin. Chem. **42**, 675 (1996)
E. Garai, S. Sensarn, C.L. Zavaleta, D. Van de Sompel, N.O. Loewke, M.J. Mandella, S.S. Gambhir, C.H. Contag, High-sensitivity, real-time, ratiometric imaging of surface-enhanced Raman scattering nanoparticles with a clinically translatable Raman endoscope device. J. Biomed. Opt. **18**, 096008 (2013)
E. Garai, S. Sensarn, C.L. Zavaleta, N.O. Loewke, S. Rogalla, M.J. Mandella, S.A. Felt, S. Friedland, J.T.C. Liu, S.S. Gambhir, C.H. Contag, A real-time clinical endoscopic system for intraluminal, multiplexed imaging of surface-enhanced Raman scattering nanoparticles. PLoS ONE **10**, e0123185 (2015)
E. Gormally, E. Caboux, P. Vineis, P. Hainaut, Circulating free DNA in plasma or serum as biomarker of carcinogenesis: Practical aspects and biological significance. Mutat. Res. Rev. Mutat. **635**, 105 (2007)
D. Graham, R. Stevenson, D.G. Thompson, L. Barrett, C. Dalton, K. Faulds, Combining functionalised nanoparticles and SERS for the detection of DNA relating to disease. Faraday Discuss. **149**, 291 (2011)
J.H. Granger, M.C. Granger, M.A. Firpo, S.J. Mulvihill, M.D. Porter, Toward development of a surface-enhanced Raman scattering (SERS)-based cancer diagnostic immunoassay panel. Analyst **138**, 410 (2013)
D.S. Grubisha, R.J. Lipert, H.Y. Park, J. Driskell, M.D. Porter, Femtomolar detection of prostate-specific antigen: an immunoassay based on surface-enhanced Raman scattering and immunogold labels. Anal. Chem. **75**, 5936 (2003)
L. Guerrini, R. Arenal, B. Mannini, F. Chiti, R. Pini, P. Matteini, R.A. Alvarez-Puebla, SERS detection of amyloid oligomers on metallorganic-decorated plasmonic beads. ACS Appl. Mater. Interfaces **7**, 9420 (2015)

V.K. Gupta, N. Atar, M.L. Yola, M. Eryilmaz, H. Torul, U. Tamer, I.H. Boyaci, Z. Üstündag, A novel glucose biosensor platform based on Ag@AuNPs modified graphene oxide nanocomposite and SERS application. J. Colloid Interf. Sci. **406**, 231 (2013)

H. Han, X. Yan, R. Dong, G. Ban, K. Li, Analysis of serum type II diabetes mellitus and diabetic complication using surface-enhanced Raman spectra (SERS). Appl. Phys. B **94**, 667 (2009)

S. Harmsen, R. Huang, M.A. Wall, H. Karabeber, J.M. Samii, M. Spaliviero, J.R. White, S. Monette, R. O'Connor, K.L. Pitter, S.A. Sastra, M. Saborowski, E.C. Holland, S. Singer, K. P. Olive, S.W. Lowe, R.G. Blasberg, M.F. Kircher, Surface-enhanced resonance Raman scattering nanostars for high-precision cancer imaging. Sci. Transl. Med. **7**, 271ra7 (2015a)

S. Harmsen, M.A. Bedics, M.A. Wall, R. Huang, M.R. Detty, M.F. Kircher, Rational design of a chalcogenopyrylium-based surface-enhanced resonance Raman scattering nanoprobe with attomolar sensitivity. Nat. Commun. **6**, 6570 (2015b)

M.M. Harper, B. Robertson, A. Ricketts, K. Faulds, Specific detection of DNA through coupling of a TaqMan assay with surface enhanced Raman scattering (SERS). Chem. Commun. **48**, 9412 (2012)

C.L. Haynes, C.R. Yonzon, X. Zhang, R.P. Van Duyne, Surface-enhanced Raman sensors: early history and the development of sensors for quantitative biowarfare agents and glucose detection. J. Raman Spectrosc. **36**, 471 (2005)

P.H. Hsu, H.K. Chiang, Surface-enhanced Raman spectroscopy for quantitative measurement of lactic acid at physiological concentration in human serum. J. Raman Spectrosc. **41**, 1610 (2010)

J. Hu, P.C. Zheng, J.H. Jiang, G.L. Shen, R.Q. Yu, G.K. Liu, Sub-attomolar HIV-1 DNA detection using surface-enhanced Raman spectroscopy. Analyst **135**, 1084 (2010)

S. Huang, L. Wang, W. Chen, S. Feng, J. Lin, Z. Huang, G. Chen, B. Li, R. Chen, Potential of non-invasive esophagus cancer detection based on urine surface-enhanced Raman spectroscopy. Laser Phys. Lett. **11**, 115604 (2014)

Y.S. Huh, A.J. Chung, B. Cordovez, D. Erickson, Enhanced on-chip SERS based biomolecular detection using electrokinetically active microwells. Lab. Chip **9**, 433 (2009)

P. Iacono, H. Karabeber, M.F. Kircher, A "schizophotonic" all-in-one nanoparticle coating for multiplexed SE(R)RS biomedical imaging. Angew. Chem. Int. Ed. **53**, 11756 (2014)

N.R. Isola, D.L. Stokes, T. Vo-Dinh, Surface enhanced Raman gene probe for HIV detection. Anal. Chem. **70**, 1352 (1998)

R.M. Jarvis, R. Goodacre, Discrimination of bacteria using surface-enhanced Raman spectroscopy. Anal. Chem. **76**, 40 (2004)

W. Jiang, B.Y.S. Kim, J.T. Rutka, W.C.W. Chan, Nanoparticle-mediated cellular response is size-dependent. Nat. Nanotechnol. **3**, 145 (2008)

J.V. Jokerst, A.J. Cole, D. Van de Sompel, S.S. Gambhir, Gold nanorods for ovarian cancer detection with photoacoustic imaging and resection guidance via Raman imaging in living mice. ACS Nano **6**, 10366 (2012)

S. Jung, J. Nam, S. Hwang, J. Park, J. Hur, K. Im, N. Park, S. Kim, Theragnostic pH-sensitive gold nanoparticles for the selective surface enhanced Raman scattering and photothermal cancer therapy. Anal. Chem. **85**, 7674 (2013)

A. Kaminska, E. Witkowska, K. Winkler, I. Dziecielewski, J.L. Weyher, J. Waluk, Detection of hepatitis B virus antigen from human blood: SERS immunoassay in a microfluidic system. Biosens. Bioelectron. **66**, 461 (2015)

T. Kang, S.M. Yoo, I. Yoon, S.Y. Lee, B. Kim, Patterned multiplex pathogen DNA detection by Au particle-on-wire SERS sensor. Nano Lett. **10**, 1189 (2010)

B. Kang, M.M. Afifi, L.A. Austin, M.A. El-Sayed, Exploiting the nanoparticle plasmon effect: observing drug delivery dynamics in single cells via Raman/fluorescence imaging spectroscopy. ACS Nano **7**, 7420 (2013)

H. Karabeber, R. Huang, P. Iacono, J.M. Samii, K. Pitter, E.C. Holland, M.F. Kircher, Guiding brain tumor resection using surface-enhanced Raman scattering nanoparticles and hand-held Raman scanner. ACS Nano **8**, 9755 (2014)

S. Keren, C.L. Zavaleta, Z. Cheng, A. de la Zerda, O. Gheysens, S.S. Gambhir, Noninvasive molecular imaging of small living subjects using Raman spectroscopy. Proc. Natl. Acad. Sci. **105**, 5844 (2008)

M.F. Kircher, A. de la Zerda, J.V. Jokerst, C.L. Zavaleta, P.J. Kempen, E. Mittra, K. Pittner, R.M. Huang, C. Campos, F. Habte, R. Sinclair, C.W. Brennan, I.K. Mellinghoff, E.C. Holland, S.S. Gambhir, A brain tumor molecular imaging strategy using a new triple-modality MRI-photoacoustic-Raman nanoparticle. Nat. Med. **18**, 829 (2012)

M. Knauer, N.P. Ivleva, X.J. Liu, R. Niessner, C. Haisch, Surface-enhanced Raman scattering-based label-free microarray readout for the detection of microorganisms. Anal. Chem. **82**, 2766 (2010)

J. Ko, S. Lee, E.K. Lee, S.I. Chang, L. Chen, S.Y. Yoon, J. Choo, SERS-based immunoassay of tumor marker VEGF using DNA aptamers and silica-encapsulated hollow gold nanospheres. Phys. Chem. Chem. Phys. **15**, 5379 (2013)

K.V. Kong, Z. Lam, W.K.O. Lau, W.K. Leong, M. Olivo, A transition metal carbonyl probe for use in a highly specific and sensitive SERS-based assay for glucose. J. Am. Chem. Soc. **135**, 18028 (2013)

R.R. Kopito, Aggresomes, inclusion bodies and protein aggregation. Trends Cell Biol. **10**, 524 (2000)

M. Lee, S. Lee, J.H. Lee, H.W. Lim, G.H. Seong, E.K. Lee, S.I. Chang, C.H. Oh, J. Choo, Highly reproducible immunoassay of cancer markers on a gold-patterned microarray chip using surface-enhanced Raman scattering imaging. Biosens. Bioelectron. **26**, 2135 (2011a)

K. Lee, V.P. Drachev, J. Irudayaraj, DNA-gold nanoparticle reversible networks grown on cell surface marker sites: application in diagnostics. ACS Nano **5**, 2109 (2011b)

S.X. Li, Q.Y. Zeng, L.F. Li, Y.J. Zhang, M.M. Wan, Z.M. Liu, H.L. Xiong, Z.Y. Guo, S.H. Liu, Study of support vector machine and serum surface-enhanced Raman spectroscopy for noninvasive esophageal cancer detection. J. Biomed. Opt. **18**, 027008 (2013)

Y. Li, X. Qi, C. Lei, Q. Yue, S. Zhang, Simultaneous SERS detection and imaging of two biomarkers on the cancer cell surface by self-assembly of branched DNA–gold nanoaggregates. Chem. Commun. **50**, 9907 (2014)

L.J. Liang, D.S. Huang, H.L. Wang, H.B. Li, S.P. Xu, Y.X. Chang, H. Li, Y.W. Yang, C.Y. Liang, W.Q. Xu, In situ surface-snhanced Raman scattering spectroscopy exploring molecular changes of drug-treated cancer cell nucleus. Anal. Chem. **87**, 2504 (2015)

C.C. Lin, Y.M. Yang, Y.F. Chen, T.S. Yang, H.C. Chang, A new protein A assay based on Raman reporter labeled immunogold nanoparticles. Biosens. Bioelectron. **24**, 178 (2008)

D. Lin, S. Feng, J. Pan, Y. Chen, J. Lin, G. Chen, S. Xie, H. Zeng, R. Chen, Colorectal cancer detection by gold nanoparticle based surface-enhanced Raman spectroscopy of blood serum and statistical analysis. Opt. Express **19**, 13565 (2011a)

J. Lin, R. Chen, S. Feng, J. Pan, Y. Li, G. Chen, M. Cheng, Z. Huang, Y. Yu, H. Zeng, A novel blood plasma analysis technique combining membrane electrophoresis with silver nanoparticle based SERS spectroscopy for potential applications in non-invasive cancer detection. Nanomed. Nanotechnol. **7**, 655 (2011b)

J. Lin, Z. Huang, S. Feng, J. Lin, N. Liu, J. Wang, L. Li, Y. Zeng, B. Li, H. Zeng, R. Chen, Label-free optical detection of type II diabetes based on surface-enhanced Raman spectroscopy and multivariate analysis. J. Raman Spectrosc. **45**, 884 (2014)

S. Link, M.A. El-Sayed, Shape and size dependence of radiative, non-radiative and photothermal properties of gold nanocrystals. Int. Rev. Phys. Chem. **19**, 409 (2000)

R. Liu, X. Zi, Y. Kang, M. Si, Y. Wu, Surface-enhanced Raman scattering study of human serum on PVA-Ag nanofilm prepared by using electrostatic self-assembly. J. Raman Spectrosc. **42**, 137 (2011)

R.M. Liu, Y. Xiong, W.Y. Tang, Y. Guo, X.H. Yan, M.Z. Si, Near-infrared surface-enhanced Raman spectroscopy (NIR-SERS) studies on oxyheamoglobin (OxyHb) of liver cancer based on PVA-Ag nanofilm. J. Raman Spectrosc. **44**, 362 (2013a)

Y. Liu, Z. Chang, H. Yuan, A.M. Fales, T. Vo-Dinh, Quintuple-modality (SERS-MRI-CT-TPL-PTT) plasmonic nanoprobe for theranostics. Nanoscale **5**, 12126 (2013b)

W.T. Lu, A.K. Singh, S.A. Khan, D. Senapati, H.T. Yu, P.C. Ray, Gold nano-popcorn-based targeted diagnosis, nanotherapy treatment, and in situ monitoring of photothermal therapy response of prostate cancer cells using surface-enhanced Raman spectroscopy. J. Am. Chem. Soc. **132**, 18103 (2010)

B. Lutz, C.E. Dentinger, L. Nguyen, L. Sun, J. Zhang, A. Allen, S. Chan, B.S. Knudsen, Spectral analysis of multiplex Raman probe signature. ACS Nano **2**, 2306 (2008)

O. Lyandres, N.C. Shah, C.R. Yonzon, J.T. Walsh, M.R. Glucksberg, R.P. Van Duyne, Real-time glucose sensing by surface-enhanced Raman spectroscopy in bovine plasma facilitated by a mixed decanethiol/mercaptohexanol partition layer. Anal. Chem. **77**, 6134 (2005)

A. MacAskill, D. Crawford, D. Graham, K. Faulds, DNA sequence detection using surface-enhanced resonance Raman spectroscopy in a homogeneous multiplexed assay. Anal. Chem. **81**, 8134 (2009)

C.M. MacLaughlin, N. Mullaithilaga, G. Yang, S.Y. Ip, C. Wang, G.C. Walker, Surface-enhanced Raman scattering dye-labeled au nanoparticles for triplexed detection of leukemia and lymphoma cells and sers flow cytometry. Langmuir **29**, 1908 (2013)

S. Mahajan, J. Richardson, T. Brown, P.N. Bartlett, SERS-melting: a new method for discriminating mutations in DNA sequences. J. Am. Chem. Soc. **130**, 15589 (2008)

K.K. Maiti, U.S. Dinish, A. Samanta, M. Vendrell, K.S. Soh, S.J. Park, M. Olivo, Y.T. Chang, Multiplex targeted in vivo cancer detection using sensitive near-infrared SERS nanotags. Nano Today **7**, 85 (2012)

N.E. Marotta, K.R. Beavers, L.A. Bottomley, Limitations of surface enhanced Raman scattering in sensing DNA hybridization demonstrated by label-free DNA oligos as molecular rulers of distance-dependent enhancement. Anal. Chem. **85**, 1440 (2013)

R. McQueenie, R. Stevenson, R. Benson, N. MacRitchie, I. McInnes, P. Maffia, K. Faulds, D. Graham, J. Brewer, P. Garside, Detection of inflammation in vivo by surface-enhanced Raman scattering provides higher sensitivity than conventional fluorescence imaging. Anal. Chem. **84**, 5968 (2012)

P.Z. McVeigh, R.J. Mallia, I. Veillieux, B.C. Wilson, Development of widefield SERS imaging endoscope. Proc. SPIE **8217**, 821704 (2012)

A.M. Mohs, M.C. Mancini, S. Singhal, J.M. Provenzale, B. Leyland-Jones, M.D. Wang, S.M. Nie, Hand-held spectroscopic device for in vivo and intraoperative tumor detection: contrast enhancement, detection sensitivity, and tissue penetration. Anal. Chem. **82**, 9058 (2010)

P. Negri, R.A. Dluhy, Detection of genetic markers related to high pathogenicity in influenza by SERS. Analyst **138**, 4877 (2013)

Z.A. Nima, M. Mahmood, Y. Xu, T. Mustafa, F. Watanabe, D.A. Nedosekin, M.A. Juratli, T. Fahmi, E.I. Galanzha, J.P. Nolan, A.G. Basnakian, V.P. Zharov, A.S. Biris, Circulating tumor cell identification by functionalized silver-gold nanorods with multicolor, super-enhanced SERS and photothermal resonances. Sci. Rep. **4**, 4752 (2014)

M.S. Noh, S. Lee, H. Kang, J.K. Yang, H. Lee, D. Hwang, J.W. Lee, S. Jeong, Y. Jang, B.H. Jun, D.H. Jeong, S.K. Kim, Y.S. Lee, M.H. Cho, Target-specific near-IR induced drug release and photothermal therapy with accumulated Au/Ag hollow nanoshells on pulmonary cancer cell membranes. Biomaterials **45**, 81 (2015)

K. Ock, W.I. Jeon, E.O. Ganbold, M. Kim, J. Park, J.H. Seo, K. Cho, S.W. Joo, S.Y. Lee, Real-time monitoring of glutathione-triggered thipurine anticancer drug release in live cells investigated by surface-enhanced Raman scattering. Anal. Chem. **84**, 2172 (2012)

J. Oh, A. Sahgal, P. Sanghera, M.N. Tsao, P. Davey, K. Lam, S. Symons, R. Aviv, J.R. Perry, Glioblastoma: patterns of recurrence and efficacy of salvage treatments. Can. J. Neurol. Sci. **38**, 621 (2011)

A. Pal, N.R. Isola, J.P. Alarie, D.L. Stokes, T. Vo-Dinh, Synthesis and characterization of SERRS gene probe for BRCA-1 (breast cancer). Faraday Discuss. **132**, 293 (2006)

W. Pang, J. Wang, R. Xiao, S. Wang, SERS molecular sentinel for the RNA genetic marker of PB1-F2 protein in highly pathogenic avian influenza (HPAI) virus. Biosens. Bioelectron. **61**, 460 (2014)

H.Y. Park, J.D. Driskell, K.M. Kwarta, R.J. Lipert, M.D. Porter, C. Schoen, J.D. Neill, J.F. Ridpath, Ultrasensitive immunoassays based on surface-enhanced Raman scattering by immunogold labels, in *Surface-Enhanced Raman Scattering: Physics and Applications,* vol. **103**, ed. by K. Kneipp, M. Moskovits, H. Kneipp (Springer, Berlin Heidelberg 2006), pp. 427–446 (Top. Appl. Phys.)

H. Park, S. Lee, L. Chen, E.K. Lee, S.Y. Shin, Y.H. Lee, S.W. Son, C.H. Oh, J.M. Song, S.H. Kang, J. Choo, SERS imaging of HER2-overexpressed MCF7 cells using antibody-conjugated gold nanorods. Phys. Chem. Chem. Phys. **11**, 7444 (2009)

I.S. Patel, W.R. Premasiri, D.T. Moir, L.D. Ziegler, Barcoding bacterial cells: a SERS-based methodology for pathogen identification. J. Raman Spectrosc. **39**, 1660 (2008)

J.H. Phan, R.A. Moffitt, T.H. Stokes, J. Liu, A.N. Young, S. Nie, M.D. Wang, Convergence of biomarkers, bioinformatics and nanotechnology for individualized cancer treatment. Trends Biotechnol. **27**, 350 (2009)

M.D. Porter, R.L. Lipert, L.M. Siperko, G. Wang, R. Narayanan, SERS as a bioassay platform: fundamentals, design and applications. Chem. Soc. Rev. **37**, 1001 (2008)

W.R. Premasiri, J.C. Lee, L.D. Ziegler, Surface-enhanced Raman scattering of whole human blood, blood plasma, and red blood cells: cellular processes and bioanalytical sensing. J. Phys. Chem. B **116**, 9376 (2012a)

W.R. Premasiri, A.F. Sauer-Budge, J.C. Lee, C.M. Klapperich, L.D. Ziegler, Rapid bacterial diagnostics via surface-enhanced Raman microscopy. Spectroscopy **27**, s8 (2012b)

W.R. Premasiri, P. Lemler, Y. Chen, Y. Gebregziabher, L.D. Ziegler, SERS analysis of bacteria, human blood and cancer cells: a metabolomic and siagnostic tool, in *Frontiers of Surface-Enhanced Raman Scattering: Single Nanoparticles and Single Cells*, ed. by Y. Ozaki, K. Kneipp, R. Aroca (Wiley, Chichester, 2014), pp. 257–283

X.M. Qian, X.H. Peng, D.O. Ansari, Q. Yin-Goen, G.Z. Chen, D.M. Shin, L. Yang, A.N. Young, M.D. Wang, S.M. Nie, In vivo tumor targeting and spectroscopic detection with surface-enhanced Raman nanoparticle tags. Nat. Biotechnol. **26**, 83 (2008)

J. Qian, L. Jiang, F. Cai, D. Wang, S. He, Fluorescence-surface enhanced Raman scattering co-functionalized gold nanorods as near-infrared probes for purely optical in vivo imaging. Biomaterials **32**, 1601 (2011)

S.P. Ravindranath, Y. Wang, J. Irudayaraj, SERS driven cross-platform based multiplex pathogen detection. Sensor Actuat. B Chem. **152**, 183 (2011)

W. Ren, Y.X. Fang, E.K. Wang, A binary functional substrate for enrichment and ultrasensitive SERS spectroscopic detection of folic acid using graphene oxide/Ag nanoparticle hybrids. ACS Nano **5**, 6425 (2011)

L. Rodríguez-Lorenzo, Z. Krpetic, S. Barbosa, R.A. Alvarez-Puebla, L.M. Liz-Marzán, I.A. Prior, M. Brust, Intracellular mapping with SERS-encoded gold nanostars. Integr. Biol. **3**, 922 (2011)

A. Samanta, K.K. Maiti, K.S. Soh, X.J. Liao, M. Vendrell, U.S. Dinish, S.W. Yun, R. Bhuvaneswari, H. Kim, S. Rautela, J.H. Chung, M. Olivo, Y.T. Chang, Ultrasensitive near-infrared Raman reporters for SERS-based in vivo cancer detection. Angew. Chem. Int. Ed. Engl. **50**, 6089 (2011)

S. Schlücker, B. Küstner, A. Punge, R. Bonfig, A. Marx, P. Ströbel, Immuno-Raman microspectroscopy: In situ detection of antigens in tissue specimens by surface-enhanced Raman scattering. J. Raman Spectrosc. **37**, 719 (2006)

V.L. Schmit, R. Martoglio, K.T. Carron, Lab-on-a-bubble surface enhanced Raman indirect immunoassay for cholera. Anal. Chem. **84**, 4233 (2012)

M. Schütz, D. Steinigeweg, M. Salehi, K. Kömpe, S. Schlücker, Hydrophilically stabilized gold nanostars as SERS labels for tissue imaging of the tumor suppressor p63 by immuno-SERS microscopy. Chem. Commun. **47**, 4216 (2011)

M.Y. Sha, H. Xu, M.J. Natan, R. Cromer, Surface-enhanced Raman scattering tags for rapid and homogeneous detection of circulating tumor cells in the presence of human whole blood. J. Am. Chem. Soc. **130**, 17214 (2008)

K.E. Shafer-Peltier, C.L. Haynes, M.R. Glucksberg, R.P. Van Duyne, Toward a glucose biosensor based on surface-enhanced Raman scattering. J. Am. Chem. Soc. **125**, 588 (2003)

N.C. Shah, O. Lyandres, J.T. Walsh, M.R. Glucksberg, R.P. Van Duyne, Lactate and sequential lactate-glucose sensing using surface-enhanced Raman spectroscopy. Anal. Chem. **79**, 6927 (2007)

W. Shi, R.J. Paproski, R. Moore, R. Zemp, Detection of circulating tumor cells using targeted surface-enhanced Raman scattering nanoparticles and magnetic enrichment. J. Biomed. Opt. **19**, 056014 (2014)

M.G. Shim, L.M. Song, N.E. Marcon, B.C. Wilson, In vivo near infrared Raman spectroscopy: demonstration of feasibility during clinical gastrointestinal endoscopy. Photochem. Photobiol. **72**, 146 (2000)

J. Song, J. Zhou, H. Duan, Self-assembled plasmonic vesicles of SERS-encoded amphiphilic gold nanoparticles for cancer cell targeting and traceable intracellular drug delivery. J. Am. Chem. Soc. **134**, 13458 (2012)

R. Stevenson, S. McAughtrie, L. Senior, R.J. Stokes, H. McGachy, L. Tetley, P. Nativo, J.M. Brewer, J. Alexander, K. Faulds, D. Graham, Analysis of intracellular enzyme activity by surface enhanced Raman scattering. Analyst **138**, 6331 (2013)

N. Stone, K. Faulds, D. Graham, P. Matousek, Prospects of deep Raman spectroscopy for noninvasive detection of conjugated surface enhanced resonance raman scattering nanoparticles buried within 25 mm of mammalian tissue. Anal. Chem. **82**, 3969 (2010)

N. Stone, M. Kerssens, G.R. Lloyd, K. Faulds, D. Graham, P. Matousek, Surface enhanced spatially offset Raman spectroscopic (SESORS) imaging—the next dimension. Chem. Sci. **2**, 776 (2011)

R. Stosch, A. Henrion, D. Schiel, B. Guttler, Surface-enhanced Raman scattering based approach for quantiative determination of creatinine in human serum. Anal. Chem. **77**, 7386 (2005)

K.K. Strelau, A. Brinker, C. Schnee, K. Weber, R. Möller, J. Popp, Detection of PCR products amplified from DNA of epizootic pathogens using magnetic nanoparticles and SERS. J. Raman Spectrosc. **42**, 243 (2011)

D.A. Stuart, C.R. Yonzon, X.Y. Zhang, O. Lyandres, N.C. Shah, M.R. Glucksberg, J.T. Walsh, R. P. Van Duyne, Glucose sensing using near-infrared surface-enhanced Raman spectroscopy: gold surfaces, 10-day stability, and improved accuracy. Anal. Chem. **77**, 4013 (2005)

D.A. Stuart, J.M. Yuen, N. Shah, O. Lyandres, C.R. Yonzon, M.R. Glucksberg, J.T. Walsh, R. P. Van Duyne, In vivo glucose measurement by surface-enhanced Raman spectroscopy. Anal. Chem. **78**, 7211 (2006)

L. Sun, J. Irudayaraj, Quantitative surface-enhanced Raman for gene expression estimation. Biophys. J. **96**, 4709 (2009)

L. Sun, K.B. Sung, C. Dentinger, B. Lutz, L. Nguyen, J. Zhang, H. Qin, M. Yamakawa, M. Cao, Y. Lu, A.J. Chmura, J. Zhu, X. Su, A.A. Berlin, S. Chan, B. Knudsen, Composite organic-inorganic nanoparticles as Raman labels for tissue analysis. Nano Lett. **7**, 351 (2007)

L. Sun, C. Yu, J. Irudayaraj, Raman multiplexers for alternative gene splicing. Anal. Chem. **80**, 3342 (2008)

A.S. Thakor, R. Paulmurugan, P. Kempen, C. Zavaleta, R. Sinclair, T.F. Massoud, S.S. Gambhir, Oxidative stress mediates the effects of Raman-active gold nanoparticles in human cells. Small **7**, 126 (2011a)

A.S. Thakor, R. Luong, R. Paulmurugan, F.I. Lin, P.Kempen, C. Zavaleta, P. Chu, T.F. Massoud, R. Sinclair, S.S. Gambhir, The fate and toxicity of Raman active silica-gold nanoparticles in mice. Sci. Transl. Med. **3**, 79ra33 (2011b)

L.M. Tian, N. Gandra, S. Singamaneni, Monitoring controlled release of payload from gold nanocages using surface enhanced Raman scattering. ASC Nano **7**, 4252 (2013)

D. van Lierop, K. Faulds, D. Graham, Separation free DNA detection using surface enhanced Raman scattering. Anal. Chem. **83**, 5817 (2011)

D. van Lierop, I.A. Larmour, K. Faulds, D. Graham, SERS primers and their mode of action for pathogen DNA detection. Anal. Chem. **85**, 1408 (2013)

T. Vo-Dinh, K. Houck, D.L. Stokes, Surface-enhanced Raman gene probes. Anal. Chem. **66**, 3379 (1994)

T. Vo-Dinh, Y. Liu, A.M. Fales, H. Ngo, H.N. Wang, J.K. Register, H. Yuan, S.J. Norton, G.D. Griffin, SERS nanosensors and nanoreporters: golden opportunities in biomedical applications. WIREs Nanomed. Nanobiotechnol. **7**, 17 (2015)

G. von Maltzahn, A. Centrone, J.H. Park, R. Ramanathan, M.J. Sailor, T.A. Hatton, S. Bhatia, SERS-coded gold nanorods as a multifunctional platform for densely multiplexed near-infrared imaging and photothermal heating. Adv. Mater. **21**, 3175 (2009)

M.B. Wabuyele, T. Vo-Dinh, Detection of human immunodeficiency virus type 1 DNA sequence using plasmonic nanoprobes. Anal. Chem. **77**, 7810 (2005)

M.B. Wabuyele, F. Yan, T. Vo-Dinh, Plasmonics nanoprobes: detection of single-nucleotide polymorphisms in the breast cancer BRCA1 gene. Anal. Bioanal. Chem. **398**, 729 (2010)

H.N. Wang, T. Vo-Dinh, Multiplex detection of breast cancer biomarkers using plasmonic molecular sentinel nanoprobes. Nanotechnology **20**, 065101 (2009)

Y.L. Wang, J.L. Seebald, D.P. Szeto, J. Irudayaraj, Biocompatibility and biodistribution of surface-enhanced Raman scattering nanoprobes in zebrafish embryos: in vivo and multiplex imaging. ACS Nano **4**, 4039 (2010a)

Z.Y. Wang, S.F. Zong, J. Yang, C.Y. Song, J. Li, Y.P. Cui, One-step functionalized gold nanorods as intracellular probe with improved SERS performance and reduced cytotoxicity. Biosens. Bioelectron. **26**, 241 (2010b)

Y.L. Wang, S. Ravindranath, J. Irudayaraj, Separation and detection of multiple pathogens in a food matrix by magnetic SERS nanoprobes. Anal. Bioanal. Chem. **399**, 1271 (2011a)

G. Wang, R.J. Lipert, M. Jain, S. Kaur, S. Chakraboty, M.P. Torres, S.K. Batra, R.E. Brand, M.D. Porter, Detection of the potential pancreatic cancer marker MUC4 in serum using surface-enhanced Raman scattering. Anal. Chem. **83**, 2554 (2011b)

X. Wang, X. Qian, J.J. Beitler, Z.G. Chen, F.R. Khuri, M.M. Lewis, H.J.C. Shin, S. Nie, D.M. Shin, Detection of circulating tumor cells in human peripheral blood using surface-enhanced Raman scattering nanoparticles. Cancer Res. **71**, 1526 (2011c)

H.N. Wang, A.M. Fales, A.K. Zaas, C.W. Woods, T. Burke, G.S. Ginsburg, T. Vo-Dinh, Surface-enhanced Raman scattering molecular sentinel nanoprobes for viral infection diagnostics. Anal. Chim. Acta **786**, 153 (2013a)

H.N. Wang, A. Dhawan, Y. Du, D. Batchelor, D.N. Leonard, V. Misra, T. Vo-Dinh, Molecular sentinel-on-chip for SERS-based biosensing. Phys. Chem. Chem. Phys. **15**, 6008 (2013b)

Y. Wang, B. Yan, L.X. Chen, SERS tags: novel optical nanoprobes for bioanalysis. Chem. Rev. **113**, 1391 (2013c)

Y. Wang, A. Khan, S.Y. Leigh, D.N. Wang, Y. Chen, D. Meza, J.T.C. Liu, Comprehensive spectral endoscopy of topically applied SERS nanoparticles in the rat esofagus. Biomed. Opt. Express **5**, 2883 (2014)

L. Wu, Z.Y. Wang, S.F. Zong, H. Chen, C.L. Wang, S.H. Xu, Y.P. Cui, Simultaneous evaluation of p53 and p21 expression level for early cancer diagnosis using SERS technique. Analyst **138**, 3450 (2013)

B.J. Yakes, R.J. Lipert, J.P. Bannantine, M.D. Porter, Detection of Mycobacterium avium subsp paratuberculosis by a sonicate immunoassay based on surface-enhanced Raman scattering. Clin. Vaccine Immunol. **15**, 227 (2008)

M.V. Yigit, L.Y. Zhu, M.A. Ifediba, Y. Zhang, K. Carr, A. Moore, Z. Medarova, Noninvasive MRI-SERS imaging in living mice using an innately bimodal nanomaterial. ACS Nano **5**, 1056 (2011)

C.R. Yonzon, O. Lyandres, N.C. Shah, J.A. Dieringer, R.P. Van Duyne, Glucose sensing with surface-enhanced Raman spectroscopy, in *Surface-Enhanced Raman Scattering: Physics and Applications*, vol. **103** ed. by K. Kneipp, M. Moskovits, H. Kneipp (Springer-Verlag, Berlin Heidelberg 2006), pp. 367–379 (Top. Appl. Phys.)

C. Zavaleta, A. de la Zerda, Z. Liu, S. Keren, Z. Cheng, M. Schipper, X. Chen, H. Dai, S.S. Gambhir, Noninvasive Raman spectroscopy in living mice for evaluation of tumor targeting with carbon nanotubes. Nano Lett. **8**, 2800 (2008)

C.L. Zavaleta, B.R. Smith, I. Walton, W. Doering, G. Davis, B. Shojaei, M.J. Natan, S.S. Gambhir, Multiplexed imaging of surface enhanced Raman scattering nanotags in living mice using noninvasive Raman spectroscopy. P. Natl. Acad. Sci. USA **106**, 13511 (2009)

C.L. Zavaleta, M.F. Kircher, S.S. Gambhir, Raman's "effect" on molecular imaging. J. Nucl. Med. **52**, 1839 (2011)

C.L. Zavaleta, E. Garai, J.T.C. Liu, S. Sensarn, M.J. Mandella, D. Van de Sompel, S. Friedland, J. Van Dam, C.H. Contag, S.S. Gambhir, A Raman-based endoscopic strategy for multiplexed molecular imaging. P. Natl. Acad. Sci. USA **110**, E2288 (2013)

H. Zhang, M.H. Harpster, H.J. Park, P.A. Johnson, Surface-enhanced Raman scattering detection of DNA derived from the West Nile virus genome using magnetic capture of Raman-active gold nanoparticles. Anal. Chem. **83**, 254 (2011)